Squaraine Dyes: Molecular Design for Different Applications and Remaining Challenges

Kristina Ilina[†,#], **William M. MacCuaig**[‡,#], **Matthew Laramie**[†,#], **Jannatun N. Jeouty**[†], **Lacey R. McNally**[*,‡], **Maged Henary**[*,†,§]

[†]Department of Chemistry, Petit Science Center, Georgia State University, 100 Piedmont Avenue SE, Atlanta, Georgia 30303, United States

[‡]Department of Bioengineering, Stephenson Cancer Center, University of Oklahoma, 173 Felgar Street, Norman, Oklahoma 73019, United States

[§]Center for Diagnostics and Therapeutics, Petit Science Center, Georgia State University, 100 Piedmont Avenue SE, Atlanta, Georgia 30303, United States

Abstract

Squaraine dyes are a class of organic dyes with strong and narrow absorption bands in the near-infrared. Despite high molar absorptivities and fluorescence quantum yields, these dyes have been less explored than other dye scaffolds due to their susceptibility to nucleophilic attack. Recent strategies in probe design including encapsulation, conjugation to biomolecules, and new synthetic modifications have seen squaraine dyes emerging into the forefront of biomedical imaging and other applications. Herein, we provide a concise overview of (1) the synthesis of symmetrical and unsymmetrical squaraine dyes, (2) the relationship between structure and photophysical properties of squaraine dyes, and (3) current applications of squaraine dyes in the literature. Given the recent successes at overcoming the limitations of squaraine dyes, they show high potential in biological imaging, in photodynamic and photothermal therapies, and as molecular sensors.

Graphical Abstract
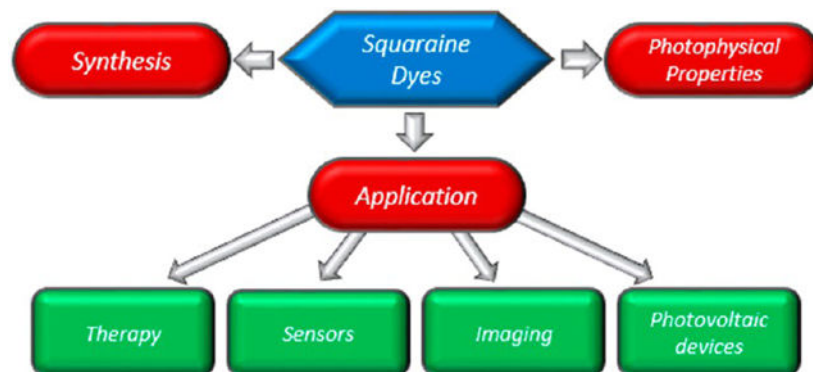
[*]**Corresponding Authors**: lacey_mcnally@hotmail.com. mhenary1@gsu.edu.
[#]K.I., W.M.M., and M.L. contributed equally to this work.

The authors declare no competing financial interest.

1. INTRODUCTION

Near infrared dyes absorb light in the range of 700–1500 nm.[1] Within this range lie the first and second therapeutic windows wherein scattering as well as absorption and autofluorescence from biomolecules are minimized allowing for increased penetration of NIR light for *in vivo* imaging and therapeutic applications. There are relatively few classes of NIR dyes that are easily synthesized or readily available, including cyanine dyes,[2–5] squaraine dyes,[6–8] phthalocyanines,[9,10] porphyrins,[11,12] and BODIPY (borondipyrromethane)[13–15] analogues.

Since cyanine dyes were first discovered by C. H. Greville Williams in 1856,[16] the cyanine class has been broadly studied for various applications, such as *in vivo* imaging, ex vivo imaging (pH sensing and DNA stains), blood spatter analysis, and solar energy conversion.[17] Cyanine dyes consist of two heteroaromic nuclei connected by an odd-numbered chain that allows for a push/pull system between the two heterocycles. The delocalization of electrons across this bridge causes them to exhibit long wavelength absorptions.[18] Monomethine and trimethine cyanine dyes absorb in the visible range, pentamethine cyanines absorb in the near-infrared region (>700 nm), and heptamethine cyanines absorb beyond 1000 nm.[19–21] These dyes are widely used in semiconducting materials, laser materials, optical recording media, paints, and biological imaging applications.[22–27]

Phthalocyanines are two-dimensional tetrapyrrolic macroheterocycles that contain 18 delocalized π-electrons, which are responsible for their intense absorption in the NIR region.[28] Phthalocyanine dyes are thermally and chemically stable and highly conjugated aromatic macrocycles that have attracted interest not only for the preparation of dyes and pigments but also as building blocks for the construction of new molecular materials for electronics and optoelectronics. In the last few years, phthalocyanines have been intensively studied as targets for optical switching and limiting devices, organic field effect transistors, sensors, light-emitting devices, low band gap molecular solar cells, optical information recording media, and photosensitizers for photodynamic therapy.[29,30]

The first member of the BODIPY dyes (the difluoroboraindacene family) was discovered by Treibs and Kreuzer in 1968.[31] This versatile class of dyes tend to be strongly UV-absorbing small molecules that emit relatively sharp fluorescence peaks with high quantum yields.[32] They have increased in popularity over the last decades thanks to their excellent thermal and photochemical stability, high fluorescence quantum yield, negligible triplet-state formation, intense absorption profile, good solubility, and chemical robustness.[33] These attractive properties make them desirable for applications as laser dyes, molecular photonic wires, chemosensors, fluorescent switches, electron transfer reagents, and bioprobes.[34]

Squaraine dyes are a class of organic dyes with an electron deficient central four-membered ring that have a resonance stabilized zwitterionic structure and were discovered by Treibs and Jacob in 1965.[35] Squaraines are derived from the highly electron deficient aromatic squaric acid core and feature electron-donating aromatic rings at diametrically opposite sides of the four-member ring. Due to their planar structures and zwitterionic properties, squaraine dyes exhibit strong absorption and emission in the NIR region. A general structure of the

squaraine chromophore is shown in Figure 1 with Ar_1 and Ar_2 generally being electron-rich anilines or heterocycles such as trimethylindolenine, benzothiazoles, and benzoselenazoles. Additionally, the squaric core can be modified by nucleophilic substitution leading to the formation of aminosquaraine and dicyanomethylene squaraine dyes.[36]

Squaraines have extremely intense absorption bands, high molar absorption coefficient, and good photoconductivity.[37–40] Squaraine dyes also tend to demonstrate a narrow absorption in the NIR range, excellent photostability,[41–43] and high quantum yield.[37] Additionally, they are prepared through a straightforward synthetic procedure.[44] Squaraine dyes can be synthesized with functional groups providing potential sites for conjugation to enhance targeting specificity without sacrificing photophysical properties.[45] Cytotoxicity studies using various squaraines[46–48] and squaraine rotaxanes[48,49] have shown that these compounds are nontoxic even at concentrations far above the therapeutic/imaging dosages, although with significant changes to the molecular structure this may change. Therefore, squaraine dyes inherently benefit from excellent photophysical and chemical properties and are adaptable to functional groups.

2. SYNTHESIS OF SQUARAINE DYES

2.1. Symmetrical Squaraine Dyes.

Symmetrical squaraine dyes consist of two of the same electron-donating groups on both sides of the oxocyclobutenolate core. The starting material for the majority of squaraine dyes syntheses is squaric acid, a colorless solid. The synthesis of symmetrical squaraines is simply the condensation of two equivalents of the aryl donor groups with a single equivalent of a squaric acid acceptor. The aryl donor groups can be pyrroles, phenols, *N,N*-dialkyl anilines, azulenes, and activated methylene heterocycles like Fisher bases, etc.[35] For the preparation of squaraine dyes, the choice of proper conditions strongly effects the success of the reaction. Initially, Treibs and Jacob used acetic anhydride in the preparation of squaraine dyes.[50] This method was later improved by Sprenger and Ziegenbein by using a one to one mixture of butanol and benzene which allowed azeotropic removal of the byproduct water and greatly improved yields.[51] This is still the preferred method of preparing squaraines although benzene has been replaced with the less toxic toluene.[52] As illustrated in Scheme 1, the synthesis of squaraine dyes begins when squaric acid is activated by alcohol and forms a "half ester" squarate, followed by active attack of a nucleophilic compound (Nu-H) and the subsequent loss of alcohol or acetic acid molecule. This leads to the formation of an intermediate semisquaraine. The next attack of nucleophile with the subsequent elimination of another alcohol or acetic acid molecule occurs at the 3-position and generating the symmetrical squaraine dye.

2.2. Unsymmetrical Squaraine Dyes.

Unsymmetrical squaraines contain two different substituents on the first and third carbons of the squaric acid moiety. There are two general synthetic routes to obtain unsymmetrical squaraine dyes, both starting from derivatives of squaric acid. The first strategy is using thionyl chloride or oxalyl chloride to prepare 3,4-dichlorocyclobut-3-ene-1,2-dione,[54] with the subsequent addition of one equivalent of an activated aromatic compound, followed by

immediate hydrolysis to obtain the intermediate semisquaraine, as shown in Scheme 2. Then the semisquaraine is then allowed to react with a different aromatic compound to afford the final unsymmetrical structure.

In the second strategy, unsymmetrical squaraine dyes containing more reactive N-alkylated heterocyclic structures such as alkyl-indolinium, alkyl-benzothiazolium, and alkyl-quinolinium salts can be synthesized through the use of 3,4-dialkoxy-cyclobut-3-ene-1,2-dione, as shown in Scheme 3.[55,56] Activated heterocyclic compounds react with 3,4-dialkoxy-cyclobut-3-ene-1,2-dione in a 1:1 ratio in ethanol with triethylamine (TEA), resulting in the semisquaraine intermediate. The semisquaraine is then reacted with another heterocyclic compound, generating the anticipated unsymmetrical structure. However, the regioselectivity should not be ignored during condensation of semisquaraine with the second equivalent of donor. During the reaction, the 1,2-condensation byproduct can be formed along with the desired 1,3-condensation product.[57]

2.3. Core-Substituted Squaraine Dyes.

Aminosquaraines are a class of squaraine dyes bearing an amino group replacing one oxygen atom of the central squaric ring. In 1998, Kim et al.[58] demonstrated that squaric acid derivatives could react with nucleophilic amines at room temperature to produce the amine substituted squaric acid from which the standard reaction pathways could be used to generate novel squaraine dyes functionalized with an alkylamino group on the squaric core (aminosquaraines). The synthesis is shown in Scheme 4.

Later, a new method was developed that involves methylation of an oxygen in the squaric acid core of the standard squaraine dye. The starting squaraine was prepared by the condensation of 2-methylbenzothiazolium salt with squaric acid and then subsequent methylation with methyl triflate, with the following nucleophilic displacement of the formed methoxy group with an aliphatic amine generating the aminosquaraine dye (Scheme 4).[59]

The different nucleophilicities of the substituting amines play a role in the variability of yields. Moreover, some of the amines may contribute to the formation of undesirable byproducts therefore decreasing the reaction yields.[60]

Another type of zwitterionic core-substituted derivative was developed by Tatarets and Terpetschnig,[61] who found that the benzothiazole- and trimethylindolenine-derived semisquarates could be easily functionalized with electron acceptors on the squaric acid core as highlighted in Scheme 5. These substituted semisquaraines can then subsequently react with a second equivalent of the heterocyclic salt at room temperature with an acceptable yield.[62]

The dicyanomethylene group was found to be the most versatile acceptor group and enabled various modifications at the donor moiety of the squaraine scaffold, leading to an extended series of dicyanomethylene-functionalized squaraines being synthesized as shown in Scheme 6.[63] Symmetrical dicyanomethylene-substituted squaraine dye synthesis includes the reaction of squaric acid and excess of n-butanol to afford the ester, which is subsequently treated with malononitrile in benzene and triethylamine. Finally, the N-alkylated

heterocyclic structures are added to afford the squaraine dye. Because of the strong electron-withdrawing character of the dicyanomethylene moiety, this squaric acid derivative displays a higher reactivity toward a huge variety of nucleophilic methylene bases than other squaric acid derivatives do.[7]

3.   PHOTOPHYSICAL PROPERTIES OF SQUARAINE DYES

3.1.   Effect of the Heterocycle Moiety and Squaric Core Nature on the Properties of Dyes.

The nature of groups (electron-donating or -withdrawing) attached to the central squarate moiety play a major role in the photophysical properties of the dye as illustrated in Table 1. Extending the π-conjugation via the heterocycles, introduction of sulfur or selenium into the conjugated backbone, introduction of halogens, and the symmetrical or unsymmetrical nature of the dyes resulted in spectral shifts in both absorption and emission.[7,64,65] Variable dyes in nonpolar solvents, such as toluene and chloroform, were analyzed below.

The absorption and fluorescence properties of the squaraine dyes showed absorption band maxima in range 628–704 nm and fluorescence band maxima in range 656–724 nm in chloroform solutions.

Dyes **2**, **3**, and **4** are unsymmetrical dyes, and differ by the halogen incorporated into one of the two conjugation branches of aniline-based squaraines. It is clear that the sharp and intense absorption bands of both halogenated squaraines are mainly located outside of the phototherapeutic window, with the absorption maximum at 632 and 635 nm. As a result of the heavy atom effect, the fluorescence quantum yields of halogenated dyes **3** and **4** are lower than that of dye **2**, particularly in the case of iodinated squaraine, suggesting that it might have a high efficiency of intersystem crossing.[67]

Modification of the alkyl chain in the squaraine dye is a commonly used method of altering photophysical properties. Condensation of the original squaric acid with malononitrile is a common technique to increase the reactivity of the squaraine core toward nucleophilic methylene bases such as indolinium salts that help in spectral tuning.[7] The dicyanomethylene addition, itself, results in a notable bathochromic shift in the spectrum as it locks the central squarate moiety into a *cis* configuration.[64] The symmetrical indolenine derivative **5** has the lowest maximum absorption wavelength (665 nm), highest molar absorptivity, and lowest fluorescence quantum yield. Although dicyanomethylene squaraines **5**–**8** show similar high extinction coefficients and maximum absorption wavelengths in the range 665–700 nm, the benzothiazole and benzoselenazole derivatives (**6**–**8**) present higher fluorescence intensities and quantum yields, probably due to the sulfur or selenium atoms in the structure.[68] Dye **8** also presents a bathochromic absorption, indicating more delocalized electronic structure due to the sulfur atom and symmetric nature of the dye.[69]

Table 2 summarizes the photophysical properties of several squaraine dyes in a polar aprotic solvent (dichloromethane).

Starting with the weakest donor benzoxazole **9** (626 nm), the increase of the donor strength via benzothiazole **12** (701 nm) up to benzoselenazole **11** (719 nm) affords a bathochromic

shift of the absorption maximum by 90 nm. The further notable bathochromic shift of the absorption maximum of more than 870 nm is achieved by changing the donor moieties to 4-methylquinolinium (**14**–**16**). Appropriately positioned substituents such as halogens at the 7-position of the quinoline donors lead to a further bathochromic shift to around 900 nm (**16**) and molar absorption coefficients above 200 000 $M^{-1} \cdot cm^{-1}$. The absorption spectra of this series of dyes illustrate that by adequate variation of donor units, a broad spectral range from 626 nm (**9**) up to 900 nm (**16**) can be covered by squaraine dyes.[63]

Particularly, the simple substitution of a hydrogen atom with increasingly heavy halogen atoms (Br, I) results in bathochromic shift of the absorption and emission spectra. This effect could be further exploited, along with other conjugation extension techniques, to yield bathochromic shifts in spectral properties, with positive effects to absorption and quantum yield.[7]

The highest fluorescence quantum yields are observed for dyes with benzoxazole (**9**), benzothiazole (**10**), and benzoselenazole (**11**). Even after adding an extra benzyl group, squaraine **12** still exhibits high fluorescence quantum yield.

3.2. Issues and Limitations of Squaraine Dyes.

Squaraine dyes are limited by toxicity, solubility, and stability in aqueous environments, as well aggregation of dye, which results in fluorescence quenching.[45] The highly electron deficient nature of the central ring of the squaraine makes the compound quite susceptible to nucleophilic attack, thus diminishing potential applications *in vivo*. Furthermore, the large, planar, and hydrophobic nature of the structure results in aggregation of the dyes in polar solutions, thus quenching fluorescence emission.

While encapsulation of the squaraine dye within micelles[71] or liposomes[72] as a method to prevent nucleophilic attack and aggregation has shown some effectiveness, alternative synthetic options have also been investigated, such as preparing the squaraines with rotaxanes (Figure 2).[73] Each of these methods provides the center squaric acid with protection from nucleophilic attack, while the nonpolar nature or bulkiness of the encapsulation prohibits the possibility of aggregate formation. Novel squaraine probes have been synthesized bypassing solubility issues, showing potential for high-performance NIR imaging.[74,75]

In addition to tuning the photophysical properties of the dye, structural manipulation can also be used to improve the biocompatibility of squaraine dyes. The inclusion of charged sulfonate groups has improved water solubility, resulting in dyes that were fully soluble in PBS solution with absorption at 775 nm.[76] Furthermore, the inclusion of reactive carboxylic acid groups or azides and alkynes for click chemistry on squarine rotaxanes has allowed the conjugation of targeting ligands. Notably, the conjugation of squaraine dyes with proteins results in large red shifts and improved quantum yields.[77] After the development of the robust, high-yielding methods for bioconjugation, squaraine rotaxanes have been employed as versatile fluorescent molecular probes for optical bioimaging.[78]

4. APPLICATION OF SQUARAINE DYES

Squaraine dyes have found wide applicability in numerous fields due to their appealing optical properties. Squaraines that undergo efficient intersystem crossing or vibrational relaxation have been employed in photodynamic and photothermal therapy. Fluorescent squaraines have been investigated for biomedical imaging and as sensors for specific analytes. Each of these applications will be discussed in the following sections.

4.1. Application of Squaraine Dyes in Therapy.

4.1.1. Photodynamic Therapy.—Photodynamic therapy (PDT) is a light-based therapy that is based on light-induced activation of a photosensitizer that generates highly reactive oxygen species to induce tissue destruction in malignant regions.[79] Two mechanisms of action for photodynamic therapy exist: type 1, production of reactive oxygen species through electron transfer, and type 2, production of singlet oxygen through electron spin change. Squaraine dyes have become intriguing photosensitizer candidates for photodynamic therapy (PDT), due to high levels of photocytotoxicity with no signs of photomutagenesis.[80]

Ramaiah et al. tested a series of halogenated and nonhalogenated squaraines in phototherapeutic applications shown in Figure 3.[80] These dyes had been previously reported; however, the mechanism of their phototoxicity was unknown. Testing with a series of additives that would block either type 1 or type 2 processes revealed that this series of squaraines proceeded through the type 2 process and damage DNA by producing singlet oxygen. Furthermore, they tested the photocytotoxicity for the series and found that brominated compound **17** showed the greatest toxicity upon visible light irradiation, especially in D_2O, which extends the lifetime of singlet oxygen relative to water.

Bagchi et al. reported the synthesis of a squaraine dye/zinc oxide nanohybrid for photodynamic therapy as shown in Figure 4.[81] They utilized zinc oxide nanoparticles both to overcome the aqueous aggregation behavior of their squaraine photosensitizer **20** and to improve the drug efficacy. The nanoparticles enhanced the toxicity relative to the squaraine alone through two proposed behaviors: first, the nanoparticles precipitate in acidic media, namely, the acidic microenvironment of tumors, enhancing drug delivery; second, the nanoparticles act as an excited state electron acceptor, increasing the generation of reactive oxygen species versus the parent squaraine dye. Though it was not directly tested, it is likely that these nanohybrids undergo type 1 processes through excited state electron transfer to produce reactive oxygen species.

Lima et al. have reported the synthesis of a series of squaraine dyes with substitutions of the central oxygen atoms and their evaluation as phototherapeutic agents.[82] They compared the efficacy of the parent squaraine **21** against the thio-, dithio-, methylamino-, dimethylamino-, and barbituric acid substituted compounds (**22**–**26**, respectively) to determine the effect of these substitutions on singlet oxygen production. They evaluated these dyes in a 1,3-diphenylisobenzofuran (DPBF) test, where absorbance of DPBF is reduced by its reaction with singlet oxygen, and used the FDA approved dye methylene blue (MB) as a control (Figure 5). Unfortunately, the DPBF test showed that only dithiosquaraine **23** displayed

comparable singlet oxygen production to the parent squaraine. Due to a vast difference in photostability, the parent squaraine showed the highest potential as a PDT therapeutic.

4.1.2. Photothermal Therapy.—Photothermal therapy (PTT) is a newly developed and encouraging therapeutic strategy that employs near-infrared (NIR) laser photoabsorbers that relax through vibrational pathways. Vibrational relaxations lead to intermolecular friction and the generation of localized heating upon laser radiation. This localized hyperthermia allows the thermal ablation of cancer cells upon NIR laser irradiation.[83–85] This offers an advantage over photodynamic therapy in that tumor hypoxia, which weakens the effectiveness of photodynamic therapy, has no such effect on photothermal therapeutics.[86] Additionally, while PDT kills cells largely through apoptotic pathways,[87] PTT can lead to large amounts of necrosis,[86] which recent reports have indicated may be more effective in treating tumors as it avoids the development of drug resistance and may increase immune response against tumor cells.[88]

Sun et al. have developed squaraine dye **27** (Figure 6), which is capable of forming brightly fluorescent J-aggregates.[89] Their goal was to develop a squaraine dye capable of imaging in the NIR-II region from 1000 to 1700 nm to take advantage of the reduced light scattering in that region of the spectrum. Using bispyrrole electron donors around the central squaraine core, they were able to obtain a dye that formed J-nanoaggregates with absorbance and fluorescence maxima at 901 and 1036 nm, respectively. *In vivo* evaluation showed that not only were these nanoaggregates capable of localizing in tumors and allowing high resolution imaging but they were also capable of inducing local hyperthermia.

Gao et al.[90] reported the synthesis of dicyanomethylene-substituted squaraine **28**, which they complexed with bovine serum albumin (BSA) for combined imaging and PTT. The BSA dye complex alleviated the normal aggregation-induced quenching in aqueous media, allowing the squaraine to be brightly fluorescent under physiological conditions. To target tumors, they conjugated folic acid to the complex, as folate receptor is overexpressed in many human cancers. In PTT assays *in vitro* against the KB carcinoma cell line, both the folic acid conjugated and nonconjugated complexes displayed greater toxicity with laser irradiation than in the dark; however, the nontargeted complex showed greater overall light toxicity as shown in Figure 7.

4.2. Application of Squaraine Dyes in Bioimaging.

The use of dyes in medical imaging has seen surging interest in recent decades, and along with other dyes scaffolds, squaraine dyes have been investigated for *in vivo* imaging applications. For bioimaging applications, the squaraine dye must be delivered to the specific type of tissue being imaged. In order to utilize the squaraine core for imaging, two distinct approaches have been attempted, namely, conjugation with a targeting ligand and encapsulation in nanostructures. The choice between these two approaches is largely influenced by how the probe is to function. Conjugation to a targeting ligand allows for multiple signaling strategies. Dyes can be attached to enzyme labile quenching groups which are cleaved under particular cellular conditions to restore signal.[91] Similarly, multiple dyes can be attached to a single targeting ligand to utilize dye aggregation as a means of signal

generation.[92] Encapsulation within nanostructures presents fewer signaling options and largely relies on the enhanced permeability and retention effect to deliver dyes to tumors. [93,94] That being said, encapsulation of squaraine dyes within nanoparticles or proteins has favorable effects on the photophysical properties of the dyes. Largely, association with nanoparticles or proteins leads to red-shifting of the absorption and emission of the dyes as well as increasing the quantum yield of fluorescence.[95–97] Ultimately, both strategies have led to effective molecular probes for biomedical imaging applications.

4.2.1. Bioconjugated Squaraine Dyes.—Saikiran et al. developed a turn-on sensor for human neutrophil elastase (HNE) detection using a dimerized squaraine dye linked by a BAla-Ala-Pro-Ala-Lys-(Obzl) peptide.[91] Specifically, elastase recognizes and hydrolyzes the Ala-Pro-Ala sequence of the peptide. In aqueous solution, the dyes' fluorescence is quenched either through aggregation- or FRET-based quenching mechanisms, but after the peptide sequence has been cleaved by elastase, the dyes are freed and fluorescence is restored as illustrated in Figure 8. Furthermore, by deprotecting the benzyl group on the terminal carboxylate, a reactive handle can be generated, which would allow for covalent linkage of the probe to glass surfaces. As such, this probe could be easily applied for point-of-care diagnostics applications.

Shimi et al.[98] synthesized a series of symmetrical (**30R**) and asymmetrical (**31R**) carbohydrate-appended squaraines for tumor targeting shown in Figure 9. The design of these probes was to take advantage of the Warburg effect, namely, that cancer cells consume and metabolize glucose at a much higher rate than normal cells.[98] Compared to the β-glucose, α-manose, and α-galactose control probes, both of the glucose-appended probes showed excellent uptake through glucose transport proteins and brightly labeled cancerous cells as shown in Figure 9. These probes also take advantage of aggregation induced quenching to enhance signal. In aqueous media, the probes aggregate, thus quenching fluorescence. After cellular uptake through glucose transporter proteins, the glucose moieties are phosphorylated by hexokinase as verified by mass spectral analysis of cell lysate. Phosphorylation drives disassembly of the aggregates and restoration of fluorescence, enabling bright signal from tumor cells.

Podgorski et al. examined a series of commercial squaraines and squaraine–rotaxanes for potential use in two-photon microscopy.[48] From the series, they identified SeTau-647 as a promising lead as it has a higher two-photon cross-section in the NIR region than rhodamine B and green fluorescent protein, which are commonly used in two-photon microscopy. In addition to its higher cross section, it was found that SeTau-647 showed strong intracellular stability and resistance to photo-bleaching. To prove the efficacy of SeTau-647, it was conjugated to a peptide (Arg-Gly-Gly-Gly-Arg-Val-Arg-Leu-Gln-Thr-Ser-Val) that has high affinity to the postsynaptic protein PSD-95, and the conjugate was used to label live tadpole neurons. After electroporation staining with the SeTau conjugate, punctate staining was observed that colocalized with immunostaining, confirming PSD-95 staining as shown in Figure 10. The neurons labeled with the SeTau conjugate were found to exhibit normal growth after staining and displayed strong fluorescence even 5 days after staining.

Karpenko et al. developed a squaraine-based probe with wide applicability based on polarity sensing.[99] Their probe was designed by conjugating two squaraines to a single targeting ligand, carbetocin (CBT), an oxytocin receptor ligand as shown in Figure 11. In aqueous media, the two dyes aggregate and quench fluorescence. When the targeting ligand binds to oxytocin, the two dyes bury into the hydrophobic cell membrane and the aggregate disassembles, restoring the fluorescence signal. Addition of excess carbetocin induced the release of the probe from the oxytocin receptor and requenching of the fluorescence as the dimer reformed. This design strategy has wide applicability as the carbetocin targeting ligand could, in theory, be replaced with any cell surface receptor ligand and still maintain the functionality of the probe.

Shaw et al.[100] developed a method to functionalize the surface of liposomes by conjugating squaraine dye CSP to cholesterol, which anchors it into the lipid bilayer of liposomes. Subsequent treatment with functionalized rotaxanes enabled specific targeting of biological structures.[100] Because the labels are added after addition of the squaraine to the liposomes, a wide variety of targeting modifications are enabled. Additionally, the PEG chains attached to squaraine **35** used to anchor the rotaxane can be lengthened or shortened to fine-tune the pharmacological properties of the liposomes. In this report, cationic Zn^{2+} dipicolylamine groups on the rotaxane were used to target bacterial cell membranes with high negative charge. In *in vitro* experiments, the targeted liposomes were found to selectively target bacterial cell membranes, even in the presence of human cells as shown in Figure 12. As the rotaxane itself is the targeting molecule, the squaraine labeled nanoparticles could be used for a myriad of applications by substituting different rotaxanes

4.2.2. Encapsulated Squaraine Dyes.

An et al. reported the use of squaraines for photoacoustic tomography using albumin as a protective carrier.[101] Before complexation with albumin, squaraine dye **36** showed a sharp absorption peak at 632 nm in organic solvent, falling outside of the NIR region. The dye–albumin complex, however, displayed a broad absorption spectrum stretching from 500 to 800 nm, well into the NIR. For *in vivo* imaging applications, several excitation wavelengths from 532 to 800 nm were tested, and the longer wavelengths improved the signal-to-noise ratio significantly, showing the advantage offered by the nanocomplex over the free dye. Finally, *in vivo* tumor imaging of 4T1 breast tumor model was performed as shown in Figure 13. Strong signal was observed from the treated mouse, while the untreated control tumor was almost indistinguishable from healthy tissues.

Sreejith et al. prepared micelle encapsulated squaraine **37** for use in dual-modal biomedical imaging with fluorescence and optoacoustic detection.[71] Use of the biocompatible surfactant Pluronic F-127 resulted in a nontoxic probe that could be further functionalized for specific imaging applications. Preliminary imaging studies in mice showed a clear enhancement of both fluorescent and optoacoustic contrast after injection of the nontargeted micelles. Before and 35 min after injection of the micelles, sequential transverse optoacoustic images were captured along a distance of 150 mm shown in the schematic in Figure 14a. Prior to injection of the micelles, no clear contrast can be seen (Figure 14c); however, the postinjection images show clear contrast enhancement in the mouse abdomen (Figure 14d).

Because the micelles contained no targeting functionalities, no specific organ targeting or uptake was described.

Zhang et al. have reported a similar liposome encapsulation of dicyanomethylene squaraine **28**.[102] By confining the dye within the phospholipid bilayer of liposomes, they were able to achieve a mixture of monomers and H-aggregates, which enabled fluorescence and optoacoustic imaging, respectively. They further utilized the enhanced permeability and retention effect of the liposomes to image MCF-7 xenograft tumors in mice as highlighted in Figure 15. The liposome encapsulated dye enabled efficient bimodal imaging of the tumors 4 h post-injection.

4.3. Applications of Squaraine Dyes as Sensors.

In addition to biomedical applications, squaraines have been employed as sensors for the detection of trace amounts of specific analytes. Their strong absorption and emission enable the development of highly responsive probes to detect metal ions, explosives, and other important molecules.

Xu et al. prepared squaraine **38**, which they have employed as a sensor for Hg^{2+} ions.[103] Alone, the dye shows very weak response to the presence of metal ions; however, in the presence of cucurbit[8]uril, a strong effect is observed with Hg^{2+} ions. Upon addition of mercury ions and the cucurbituril macrocycle, the absorbance peaks of the squaraine at 600 and 655 nm undergo a hypochromic shift, and there is a strong quenching of fluorescence. Molecular modeling studies indicate that the metal ion and squaraine both are trapped within the macrocycle, with the metal ion chelated between two of the urenyl carbonyl groups of the macrocycle and the sulfur of the squaraine benzothiazole as shown in Figure 16. Unfortunately, both Fe^{3+} and Cr^{3+} show similar quenching effects.

Wang et al. synthesized squaraine **39**, which showed selective spectral responses to the presence of Cu^{2+} ions.[104] While other metal ions led to only minute spectral changes, the addition of copper(II) ions lead to a decrease in absorbance at 514 nm and the formation of a new peak at 675 nm with an isosbestic point at 565 nm (Figure 17). The binding to Cu^{2+} was not disturbed by the presence of other metal ions, and a Job plot revealed the binding stoichiometry to be 1:1. Naked eye detection enabled the determination of Cu^{2+} ions at concentrations as low as 3 μM.

Xu et al. developed a dansylamide functionalized squaraine **40** for the detection of trace amounts of picric acid, a pollutant and explosive chemical.[105] Their sensor had a limit of detection of 70 nM picric acid. Upon interaction with picric acid, protonation of the dansyl dimethylamino group blocks the internal charge transfer pathway that gives **40** its spectral properties. This results in the decrease in the absorbance peak at 663 nm and the formation of a new peak at 627 nm with an isosbestic point at 641 nm. Similarly, the fluorescence peak at 684 nm is replaced with a new peak forming at 644 nm as shown in Figure 18.

5. CONCLUSIONS

Squaraine dyes have been shown to exhibit excellent photophysical and chemical, properties, allowing them to be suitable for applications spanning from therapy to imaging. High absorbance, quantum yield, and photostability are some of the many favorable properties possessed by squaraines. Furthermore, due to the intrinsic ability of squaraines to absorb NIR light, *in vivo* injection of a dye provides a noninvasive method to observe biological function and anatomic detail. NIR light will not harm the patient as UV or visible light would, and because competing absorbance, autofluorescence, and scattering are minimized in the NIR, the depth of penetration is greatly increased. These qualities combined with simple synthesis and tunable properties result in squaraine dye derivatives having high potential commercially and clinically.

While squaraine dyes have been and will continue to be useful for photovoltaic applications, prominent roles for squaraine dyes have emerged in the field of imaging and therapy. The coupling of high photostability with low cytotoxicity intrinsic to squaraine dyes[71] and NIR imaging could potentially allow for a noninvasive, real-time, targeting method in clinical applications. For example, a cancer-cell targeted squaraine probe may be applied *in vivo* during surgery to ensure proper removal of cancerous tissue with little to no side effects suffered, making the possibility of adopting squaraine clinically and commercially very intriguing. Advances in protecting the nucleophile sensitive central cyclooxybutenoate ring have largely overcome the problematic decomposition of squaraine dyes in biological media allowing these dyes to be used in a wide variety of biomedical imaging applications; however, the problematic solubility of squaraines remains. The vast majority of the squaraines described above remain poorly water-soluble and require solubilizing ligands or encapsulation to be compatible with biological media. Furthermore, while encapsulation within nanoparticles or rotaxanes have improved the chemical stability of these dyes, the large molecular size of these protecting groups does somewhat reduce the applicability of the final dye.

ACKNOWLEDGMENTS

REFERENCES

(1). Luo S, Zhang E, Su Y, Cheng T, and Shi C (2011) A review of NIR dyes in cancer targeting and imaging. Biomaterials 32 (29), 7127–7138. [PubMed: 21724249]

(2). Li P, Liu Y, Liu W, Li G, Tang Q, Zhang Q, Leng F, Sheng F, Hu C, Lai W, et al. (2019) IR-783 inhibits breast cancer cell proliferation and migration by inducing mitochondrial fission. Int. J. Oncol 55 (2), 415–424. [PubMed: 31173174]

(3). Figueras E, Martins A, Borbély A, Le Joncour V, Cordella P, Perego R, Modena D, Pagani P, Esposito S, Auciello G, et al. (2019) Octreotide conjugates for tumor targeting and imaging. Pharmaceutics 11 (5), 220–234.

(4). Duan L, Wang L, Zhang C, Yu L, Guo F, Sun Z, Xu Y, and Yan F (2019) Role of near-infrared heptamethine cyanine dye IR-783 in diagnosis of cervical cancer and its mechanism. Int. J. Clin. Exp. Pathol 12 (6), 2353–2362. [PubMed: 31934062]

(5). Henary M, Paranjpe S, and Owens EA (2013) Synthesis and applications of benzothiazole containing cyanine dyes. Heterocycl. Commun 19 (1), 1–11.

(6). Delcamp JH, Shi Y, Yum JH, Sajoto T, Dell'Orto E, Barlow S, Nazeeruddin MK, Marder SR, and Gratzel M (2013) The role of pi bridges in high-efficiency DSCs based on unsymmetrical squaraines. Chem. - Eur. J 19 (5), 1819–27. [PubMed: 23255425]

(7). Mayerhöffer U, Fimmel B, and Würthner F (2012) Bright Near Infrared Fluorophores Based on Squaraines by Unexpected Halogen Effects. Angew. Chem., Int. Ed 51 (1), 164–167.

(8). Wu N, Lan J, Yan L, and You J (2014) A sensitive colorimetric and fluorescent sensor based on imidazolium-functionalized squaraines for the detection of GTP and alkaline phosphatase in aqueous solution. Chem. Commun. (Cambridge, U. K.) 50 (34), 4438–41.

(9). Zink-Lorre N, Font-Sanchis E, Seetharaman S, Karr PA, Sastre-Santos Á, D'Souza F, and Fernández-Lázaro F (2019) Directly linked zinc phthalocyanine-perylenediimide dyads and a triad for ultrafast charge separation. Chem. - Eur. J 25, 10123. [PubMed: 31264744]

(10). Abrahamse H, and Houreld NN (2019) Genetic aberrations associated with photodynamic therapy in colorectal cancer cells. Int. J. Mol. Sci 20 (13), 3254.

(11). Zenkevich E, Sagun E, Knyukshto V, Shulga A, Mironov A, Efremova O, Bonnett R, Songca SP, and Kassem M (1996) Photophysical and photochemical properties of potential porphyrin an dchlorin photosensitizers for PDT. J. Photochem. Photobiol., B 33 (2), 171–180.

(12). Finlay JC, Conover DL, Hull EL, and Foster TH (2001) Porphyrin bleaching and PDT-induced spectral changes are irradiance dependent in ALA-sensitized normal rat skin *in vivo*. Photochem. Photobiol 73, 54–63. [PubMed: 11202366]

(13). Cakmak Y, and Akkaya EU (2009) Phenylethynyl-BODIPY oligomers: bright dyes and fluorescent building blocks. Org. Lett 11 (1), 85–8. [PubMed: 19053800]

(14). Chen J, Mizumura M, Shinokubo H, and Osuka A (2009) Functionalization of boron dipyrrin (BODIPY) dyes through iridium and rhodium catalysis: a complementary approach to alpha- and beta-substituted BODIPYs. Chem. - Eur. J 15 (24), 5942–9. [PubMed: 19418518]

(15). Wu L, and Burgess K (2008) A new synthesis of symmetric boraindacene (BODIPY) dyes. Chem. Commun. (Cambridge, U. K.) 40, 4933–5.

(16). Williams CG (1857) XXVI.-Researches on chinoline and its homologues. Trans. - R. Soc. Edinburgh 21, 377.

(17). Dost TL, Gressel MT, and Henary M (2017) Synthesis and Optical Properties of Pentamethine Cyanine Dyes With Carboxylic Acid Moieties. Anal. Chem. Insights 12, 1177390117711938. [PubMed: 28607539]

(18). Soriano E, Holder C, Levitz A, and Henary M (2016) Benz[c,d]indolium-containing Monomethine Cyanine Dyes: Synthesis and Photophysical Properties. Molecules 21, 23.

(19). Ballou B, Ernst LA, and Waggoner AS (2005) Fluorescence imaging of tumors in vivo. Curr. Med. Chem 12 (7), 795–805. [PubMed: 15853712]

(20). Lavis LD, and Raines RT (2008) Bright ideas for chemical biology. ACS Chem. Biol 3 (3), 142–155. [PubMed: 18355003]

(21). Lee H, Berezin MY, Henary M, Strekowski L, and Achilefu S (2008) Fluorescence lifetime properties of near-infrared cyanine dyes in relation to their structures. J. Photochem. Photobiol., A 200 (2–3), 438–444.

(22). Kusano M, Tajima Y, Yamazaki K, Kato M, Watanabe M, and Miwa M (2008) Sentinel node mapping guided by indocyanine green fluorescence imaging: a new method for sentinel node navigation surgery in gastrointestinal cancer. Dig. Surg 25 (2), 103–108. [PubMed: 18379188]

(23). Ishizawa T, Fukushima N, Shibahara J, Masuda K, Tamura S, Aoki T, Hasegawa K, Beck Y, Fukayama M, and Kokudo N (2009) Real-time identification of liver cancers by using indocyanine green fluorescent imaging. Cancer 115 (11), 2491–2504. [PubMed: 19326450]

(24). Landsman ML, Kwant G, Mook GA, and Zijlstra WG (1976) Light-absorbing properties, stability, and spectral stabilization of indocyanine green. J. Appl. Physiol 40 (4), 575–583. [PubMed: 776922]

(25). Escobedo JO, Rusin O, Lim S, and Strongin RM (2010) NIR dyes for bioimaging applications. Curr. Opin. Chem. Biol 14 (1), 64–70. [PubMed: 19926332]

(26). Owens EA, Henary M, El Fakhri G, and Choi HS (2016) Tissue-Specific Near-Infrared Fluorescence Imaging. Acc. Chem. Res 49 (9), 1731–1740. [PubMed: 27564418]

(27). Mapp CT, Owens EA, Henary M, and Grant KB (2014) Oxidative cleavage of DNA by pentamethine carbocyanine dyes irradiated with long-wavelength visible light. Bioorg. Med. Chem. Lett 24 (1), 214–219. [PubMed: 24332091]

(28). Urbani M, Ragoussi M-E, Nazeeruddin MK, and Torres T (2019) Phthalocyanines for dye-sensitized solar cells. Coord. Chem. Rev 381, 1–64.

(29). de la Torre G, Vazquez P, Agullo-Lopez F, and Torres T (2004) Role of structural factors in the nonlinear optical properties of phthalocyanines and related compounds. Chem. Rev 104 (9), 3723–3750. [PubMed: 15352778]

(30). Claessens CG, Hahn U, and Torres T (2008) Phthalocyanines: from outstanding electronic properties to emerging applications. Chem. Rec 8 (2), 75–97. [PubMed: 18366105]

(31). Treibs A, and Kreuzer FH (1968) Difluorboryl Komplexe von Di und Tripyrrylmethenen. Liebigs Ann. 718 (1), 208–223.

(32). Loudet A, and Burgess K (2007) BODIPY dyes and their derivatives: Syntheses and spectroscopic properties. Chem. Rev 107 (11), 4891–4932. [PubMed: 17924696]

(33). Ulrich G, Ziessel R, and Harriman A (2008) The chemistry of fluorescent bodipy dyes: versatility unsurpassed. Angew. Chem., Int. Ed 47 (7), 1184–1201.

(34). Salim MM, Owens EA, Gao T, Lee JH, Hyun H, Choi HS, and Henary M (2014) Hydroxylated near-infrared BODIPY fluorophores as intracellular pH sensors. Analyst 139 (19), 4862–4873. [PubMed: 25105177]

(35). Treibs A, and Jacob K (1965) Cyclotrimethine dyes derived from squaric acid. Angew. Chem., Int. Ed. Engl 4 (8), 694–694.

(36). Griffiths J, and Park S (2002) Facile preparative redox chemistry of bis(4-dialkylaminophenyl)squaraine dyes. Tetrahedron Lett. 43 (43), 7669–7671.

(37). Oswald B, Lehmann F, Simon L, Terpetschnig E, and Wolfbeis OS (2000) Red laser-induced fluorescence energy transfer in an immunosystem. Anal. Biochem 280 (2), 272–277. [PubMed: 10790310]

(38). Gross S, and Piwnica-Worms D (2006) Molecular imaging strategies for drug discovery and development. Curr. Opin. Chem. Biol 10 (4), 334–342. [PubMed: 16822702]

(39). Keller PJ, Pampaloni F, and Stelzer EH (2006) Life sciences require the third dimension. Curr. Opin. Cell Biol 18 (1), 117–24. [PubMed: 16387486]

(40). Gayathri Devi DG, Cibin TR, Ramaiah D, and Abraham A (2008) Bis (3, 5-diiodo-2, 4, 6-trihydroxyphenyl) squaraine: A novel candidate in photodynamic therapy for skin cancer models in vivo. J. Photochem. Photobiol., B 92 (3), 153–159. [PubMed: 18653354]

(41). Wang B, Fan J, Sun S, Wang L, Song B, and Peng X (2010) 1-(Carbamoylmethyl)-3H-indolium squaraine dyes: synthesis, spectra, photo-stability and association with BSA. Dyes Pigm. 85 (1–2), 43–50.

(42). Terpetsching E, Szmacinski H, and Lakowicz JR (1993) Synthesis, spectral properties and photostabilities of symmetrical and unsymmetrical squarines; a new class of flourophores with long-wavelength exiciation and emmision. Anal. Chim. Acta 282 (3), 633–641.

(43). Arunkumar E, Fu N, and Smith BD (2006) Squaraine Derived Rotaxanes: Highly Stable, Fluorescent Near IR Dyes. Chem. -Eur. J 12 (17), 4684–4690. [PubMed: 16575935]

(44). Law KY (1993) Organic photoconductive materials: recent trends and developments. Chem. Rev 93 (1), 449–486.

(45). Sreejith S, Carol P, Chithra P, and Ajayaghosh A (2008) Squaraine dyes: a mine of molecular materials. J. Mater. Chem 18 (3), 264–274.

(46). Friães S, Silva AM, Boto RE, Ferreira D, Fernandes JR, Souto EB, Almeida P, Ferreira LFV, and Reis LV (2017) Synthesis, spectroscopic characterization and biological evaluation of unsymmetrical aminosquarylium cyanine dyes. Bioorg. Med. Chem 25, 3803–3814. [PubMed: 28571975]

(47). Soumya MS, Shafeekh KM, Das S, and Abraham A (2014) Symmetrical diiodinated squaraine as an efficient photosensitizer for PDT applications: evidence from photodynamic and toxicological aspects. Chem.-Biol. Interact 222, 44–49. [PubMed: 25168848]

(48). Podgorski K, Terpetschnig E, Klochko OP, Obukhova OM, and Haas K (2012) Ultra-Bright and - Stable Red and Near-Infrared Squaraine Fluorophores for In Vivo Two-Photon Imaging. PLoS One 7 (12), No. e51980. [PubMed: 23251670]

(49). Johnson JR, Fu N, Arunkumar E, Leevy WM, Gammon ST, Piwnica Worms D, and Smith BD (2007) Squaraine rotaxanes: superior substitutes for Cy 5 in molecular probes for near infrared fluorescence cell imaging. Angew. Chem., Int. Ed 46 (29), 5528.

(50). Treibs A, and Jacob K (1965) Cyclotrimethine Dyes Derived from Squaric Acid. Angew. Chem., Int. Ed. Engl 4 (8), 694.

(51). Sprenger H-E, and Ziegenbein W (1966) Condensation Products of Squaric Acid and Tertiary Aromatic Amines. Angew. Chem., Int. Ed. Engl 5 (10), 894.

(52). Jyothish K, Arun KT, and Ramaiah D (2004) Synthesis of novel quinaldine-based squaraine dyes: effect of substituents and role of electronic factors. Org. Lett 6 (22), 3965–3968. [PubMed: 15496075]

(53). Sprenger H-E, and Ziegenbein W (1968) Cyclobutenediylium Dyes. Angew. Chem., Int. Ed. Engl 7 (7), 530–535.

(54). Keil D, and Hartmann H (2001) Synthesis and Characterization of a New Class of Unsymmetrical Squaraine Dyes. Dyes Pigm. 49 (3), 161–179.

(55). Ohno M, Yamamoto Y, Shirasaki Y, and Eguchi S (1993) Synthesis of Squaric Acid Derivatives by Lewis Acid-Catalysed Reaction of Its Dichloride, Methyl Ester Chloride, Diehtylamide Chloride, and Ethyl Diester with Unsaturated Organosilanes: New Method for C – C Bond Formation on Cyclobutenedione. J. Chem. Soc., Perkin Trans 1 12, 263–271.

(56). Balbo Block MA, Khan A, and Hecht S (2004) Avenues into the Synthesis of Illusive Poly(m-phenylene-altsquaraine)s: Polycondensation of m-Phenylenediamines with Squaric Acid Intercepted by Intermediate Semisquaraines of Exceptionally Low Reactivity. J. Org. Chem 69 (1), 184–187. [PubMed: 14703395]

(57). Zhang Y (2013) Squaraine Dyes, Design and Synthesis for Various Functional Materials Applications, Ph.D. Thesis, University of Central Florida.

(58). Kim SH, Hwang SH, Kim JJ, Yoon CM, and Keum SR (1998) Synthesis and properties of functional aminosquarylium dyes. Dyes Pigm. 37 (2), 145–154.

(59). Reis LV, Serrano JPC, Almeida P, and Santos PF (2002) New synthetic approach to aminosquarylium cyanine dyes. Synlett 10, 1617–1620.

(60). Magalhães AF, Graca VC, Calhelha RC, Ferreira Machado IL, Vieira Ferreira LF, Ferreira ICFR, and Santos PF (2019) Synthesis, photochemical and in vitro cytotoxic evaluation of benzoselenazole-based aminosquaraines. Photochem. Photobiol. Sci 18 (2), 336–342. [PubMed: 30310913]

(61). Tatarets AL, Fedyunyaeva IA, Terpetschnig E, and Patsenker LD (2005) Synthesis of novel squaraine dyes and their intermediates. Dyes Pigm. 64 (2), 125–134.

(62). Xia GM, and Wang HM (2017) Squaraine dyes: The hierarchical synthesis and its application in optical detection. J. Photochem. Photobiol, C 31, 84–113.

(63). Mayerhoffer U, Gsanger M, Stolte M, Fimmel B, and Wurthner F (2013) Synthesis and molecular properties of acceptor-substituted squaraine dyes. Chem. - Eur. J 19 (1), 218–232. [PubMed: 23180571]

(64). Qin C, Numata Y, Zhang S, Yang X, Islam A, Zhang K, Chen H, and Han L (2014) Novel Near Infrared Squaraine Sensitizers for Stable and Efficient Dye Sensitized Solar Cells. Adv. Funct. Mater 24 (20), 3059–3066.

(65). Salice P, Arnbjerg J, Pedersen BW, Toftegaard R, Beverina L, Pagani G, and Ogilby PR (2010) Photophysics of squaraine dyes: role of charge-transfer in singlet oxygen production and removal. J. Phys. Chem. A 114 (7), 2518–2525. [PubMed: 20121177]

(66). Huang Y, Lin Q, Wu J, and Fu N (2013) Design and synthesis of a squaraine based near-infrared fluorescent probe for the ratiometric detection of Zn^{2+} ions. Dyes Pigm. 99 (3), 699–704.

(67). Luo C, Zhou Q, Jiang G, He L, Zhang B, and Wang X (2011) The synthesis and 1 O 2 photosensitization of halogenated asymmetric aniline-based squaraines. New J. Chem 35 (5), 1128–1132.

(68). Martins TD, Pacheco ML, Boto RE, Almeida P, Farinha JPS, and Reis LV (2017) Synthesis, characterization and protein-association of dicyanomethylene squaraine dyes. Dyes Pigm. 147, 120–129.

(69). Pisoni DD, Petzhold CL, de Abreu MP, Rodembusch FS, and Campo LF (2012) Synthesis, spectroscopic characterization and photophysical study of dicyanomethylene-substituted squaraine dyes. C. R. Chim 15 (5), 454–462.

(70). Cong ZX, Li YF, Xia GM, Shen S, Sun JQ, Xu KK, Jiang ZJ, Jiang LX, Chen Y, Yu QM, et al. (2019) Highly efficient crystal red fluorescent 1,2-squaraine dyes with excellent biocompatibility and bioimaging. Dyes Pigm. 162, 654–661.

(71). Sreejith S, Joseph J, Lin M, Menon NV, Borah P, Ng HJ, Loong YX, Kang Y, Yu SW-K, and Zhao Y (2015) Near-infrared squaraine dye encapsulated micelles for in vivo fluorescence and photoacoustic bimodal imaging. ACS Nano 9 (6), 5695–5704. [PubMed: 26022724]

(72). Dong S, Teo JDW, Chan LY, Lee C-LK, and Sou K (2018) Far-Red Fluorescent Liposomes for Folate Receptor-targeted Bioimaging. ACS Appl. Nano Mater 1 (3), 1009–1013.

(73). Jarvis TS, Collins CG, Dempsey JM, Oliver AG, and Smith BD (2017) Synthesis and Structure of 3, 3-Dimethylindoline Squaraine Rotaxanes. J. Org. Chem 82 (11), 5819–5825. [PubMed: 28516767]

(74). Xiong L, Ma J, Huang Y, Wang Z, and Lu Z (2017) Highly Sensitive Squaraine-Based Water-Soluble Far-Red/Near-Infrared Chromofluorogenic Thiophenol Probe. ACS Sens 2 (4), 599–605. [PubMed: 28723193]

(75). Grande V, Doria F, Freccero M, and Würthner F (2017) An Aggregating Amphiphilic Squaraine: A Light up Probe That Discriminates Parallel G Quadruplexes. Angew. Chem., Int. Ed 56 (26), 7520–7524.

(76). Umezawa K, Citterio D, and Suzuki K (2008) Water-soluble NIR fluorescent probes based on squaraine and their application for protein labeling. Anal. Sci 24 (2), 213–217. [PubMed: 18270411]

(77). Markova LI, Terpetschnig EA, and Patsenker LD (2013) Comparison of a series of hydrophilic squaraine and cyanine dyes for use as biological labels. Dyes Pigm. 99 (3), 561–570.

(78). Gassensmith JJ, Baumes JM, and Smith BD (2009) Discovery and early development of squaraine rotaxanes. Chem. Commun 42, 6329–6338.

(79). Gayathri Devi DGCT, Ramaiah D, Abraham A, and Cibin TR (2008) Bis (3, 5-diiodo-2, 4, 6-trihydroxyphenyl) squaraine: A novel candidate in photodynamic therapy for skin cancer models in vivo. J. Photochem. Photobiol., B 92, 153–159. [PubMed: 18653354]

(80). Ramaiah D, Eckert I, Arun KT, Weidenfeller L, and Epe B (2004) Squaraine dyes for photodynamic therapy: mechanism of cytotoxicity and DNA damage induced by halogenated squaraine dyes plus light (>600 nm). Photochem. Photobiol 79 (1), 99–104. [PubMed: 14974721]

(81). Bagchi D, Halder A, Debnath S, Saha P, and Kumar Pal S (2019) Exploration of interfacial dynamics in squaraine based nanohybrids for potential photodynamic action. J. Photochem. Photobiol., A 380, 111842.

(82). Lima E, Ferreira O, Gomes VSD, Santos AO, Boto RE, Fernandes JR, Almeida P, Silvestre SM, and Reis LV (2019) Synthesis and *in vitro* evaluation of the antitumoral phototherapeutic potential of squaraine cyanine dyes derived from indolenine. Dyes Pigm. 167, 98–108.

(83). Alkilany AM, Thompson LB, Boulos SP, Sisco PN, and Murphy CJ (2012) Gold nanorods: Their potential for photothermal therapeutics and drug delivery, tempered by the complexity of their biological interactions. Adv. Drug Delivery Rev 64 (2), 190–199.

(84). Shanmugam V, Selvakumar S, and Yeh CS (2014) Near-infrared light-responsive nanomaterials in cancer therapeutics. Chem. Soc. Rev 43 (17), 6254–6287. [PubMed: 24811160]

(85). Zhang Z, Wang J, and Chen C (2013) Near-infrared light-mediated nanoplatforms for cancer thermo-chemotherapy and optical imaging. Adv. Mater 25 (28), 3869–3880. [PubMed: 24048973]

(86). Melamed JR, Edelstein RS, and Day ES (2015) Elucidating the fundamental mechanisms of cell death triggered by photothermal therapy. ACS Nano 9 (1), 6–11. [PubMed: 25590560]

(87). Mroz P, Yaroslavsky A, Kharkwal GB, and Hamblin MR (2011) Cell Death Pathways in Photodynamic Therapy of Cancer. Cancers 3, 2516–2539. [PubMed: 23914299]

(88). Kim J-Y, Han J-H, Park G, Seo Y-W, Yun C-W, Lee B-C, Bae J, Moon AR, and Kim T-H (2016) Necrosis-inducing peptide has the beneficial effect on killing tumor cells through neuropilin (NRP-1) targeting. Oncotarget 7 (22), 32449–32461. [PubMed: 27083053]

(89). Sun P, Wu Q, Sun X, Miao H, Deng W, Zhang W, Fan Q, and Huang W (2018) J-Aggregate squaraine nanoparticles with bright NIR-II fluorescence for imaging guided photothermal therapy. Chem. Commun 54, 13395–13398.

(90). Gao F-P, Lin Y-X, Li L-L, Liu Y, Mayerhöffer U, Spenst P, Su J-G, Li J-Y, Würthner F, and Wang H (2014) Supramolecular adducts of squaraine and protein for noninvasive tumor imaging and photothermal therapy in vivo. Biomaterials 35 (3), 1004–1014. [PubMed: 24169004]

(91). Saikiran M, Sato D, Pandey SS, Hayase S, and Kato T (2017) Efficient near infrared fluorescence detection of elastase enzyme using peptide-bound unsymmetrical squaraine dye. Bioorg. Med. Chem. Lett 27 (17), 4024–4029. [PubMed: 28784293]

(92). Karpenko IA, Collot M, Richert L, Valencia C, Villa P, Mely Y, Hibert M, Bonnet D, and Klymchenko AS (2015) Fluorogenic Squaraine Dimers with Polarity-Sensitive Folding As Bright Far-Red Probes for Background-Free Bioimaging. J. Am. Chem. Soc 137 (1), 405–412. [PubMed: 25506627]

(93). Singh R, and Lillard JWJ (2009) Nanoparticle-based targeted drug delivery. Exp. Mol. Pathol 86, 215–223. [PubMed: 19186176]

(94). Perrault SD, Walkey C, Jennings T, Fischer HC, and Chan WCW (2009) Mediating tumor targeting efficiency of nanoparticles through design. Nano Lett. 9 (5), 1909–1915. [PubMed: 19344179]

(95). Oswald B, Patsenker L, Duschl J, Szmacinski H, Wolfbeis OS, and Terpetschnig E (1999) Synthesis, spectral properties, and detection limits of reactive squaraine dyes, a new class of diode laser compatible fluorescent protein labels. Bioconjugate Chem. 10, 925–931.

(96). Tatarets AL, Fedyunyayeva IA, Dyubko TS, Povrozin YA, Doroshenko AO, Terpetschnig E, and Patsenker LD (2006) Synthesis of water-soluble, ring-substituted squaraine dyes and their evaluation as fluorescent probes and labels. Anal. Chim. Acta 570, 214–223. [PubMed: 17723402]

(97). Terpetschnig E, Szmacinski H, Ozinskas A, and Lakowicz JR (1994) Synthesis of squaraine-N-hydroxysuccinimide esters and their biological application as long-wavelength fluorescent labels. Anal. Biochem 217, 197–204. [PubMed: 8203747]

(98). Shimi M, Sankar V, Rahim MA, Nitha P, Das S, Radhakrishnan K, and Raghu K (2017) Novel glycoconjugated squaraine dyes for selective optical imaging of cancer cells. Chem. Commun 53 (39), 5433–5436.

(99). Karpenko IA, Collot M, Richert L, Valencia C, Villa P, Mely Y, Hibert M, Bonnet D, and Klymchenko AS (2015) Fluorogenic Squaraine Dimers with Polarity-Sensitive Folding As Bright Far-Red Probes for Background-Free Bioimaging. J. Am. Chem. Soc 137, 405–412. [PubMed: 25506627]

(100). Shaw SK, Liu W, Brennan SP, Betancourt-Mendiola M. d. L., and Smith BD (2017) Non-Covalent Assembly Method that Simultaneously Endows a Liposome Surface with Targeting Ligands, Protective PEG Chains, and Deep-Red Fluorescence Reporter Groups. Chem. - Eur. J 23 (51), 12646–12654. [PubMed: 28736857]

(101). An F-F, Deng Z-J, Ye J, Zhang J-F, Yang Y-L, Li C-H, Zheng C-J, and Zhang X-H (2014) Aggregation-induced near-infrared absorption of squaraine dye in an albumin nanocomplex for photoacoustic tomography in vivo. ACS Appl. Mater. Interfaces 6 (20), 17985–17992. [PubMed: 25223319]

(102). Zhang D, Zhao YX, Qiao ZY, Mayerhöffer U, Spenst P, Li XJ, Würthner F, and Wang H (2014) Nano-confined squaraine dye assemblies: new photoacoustic and near-infrared fluorescence dual-modular imaging probes in vivo. Bioconjugate Chem. 25 (11), 2021–2029.

(103). Xu Y, Panzner MJ, Li X, Youngs WJ, and Pang Y (2010) Host–guest assembly of squaraine dye in cucurbit [8] uril: its implication in fluorescent probe for mercury ions. Chem. Commun 46 (23), 4073–4075.

(104). Wang WFA, You J, Gao G, Lan J, Chen L, and Fu A (2010) Squaraine-based colorimetric and fluorescent sensors for Cu^{2+}-specific detection and fluorescence imaging in living cells. Tetrahedron 66 (21), 3695–3701.

(105). Xu Y, Li B, Li W, Zhao J, Sun S, and Pang Y (2013) "ICT-not-quenching" near infrared ratiometric fluorescent detection of picric acid in aqueous media. Chem. Commun 49 (42), 4764–4766.
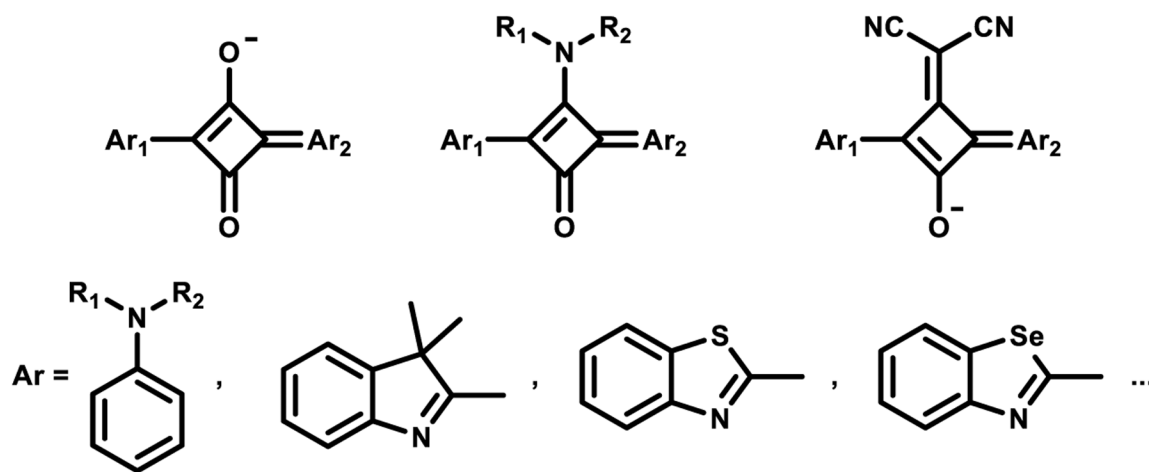
Figure 1.
Common structure of squaraine dyes.
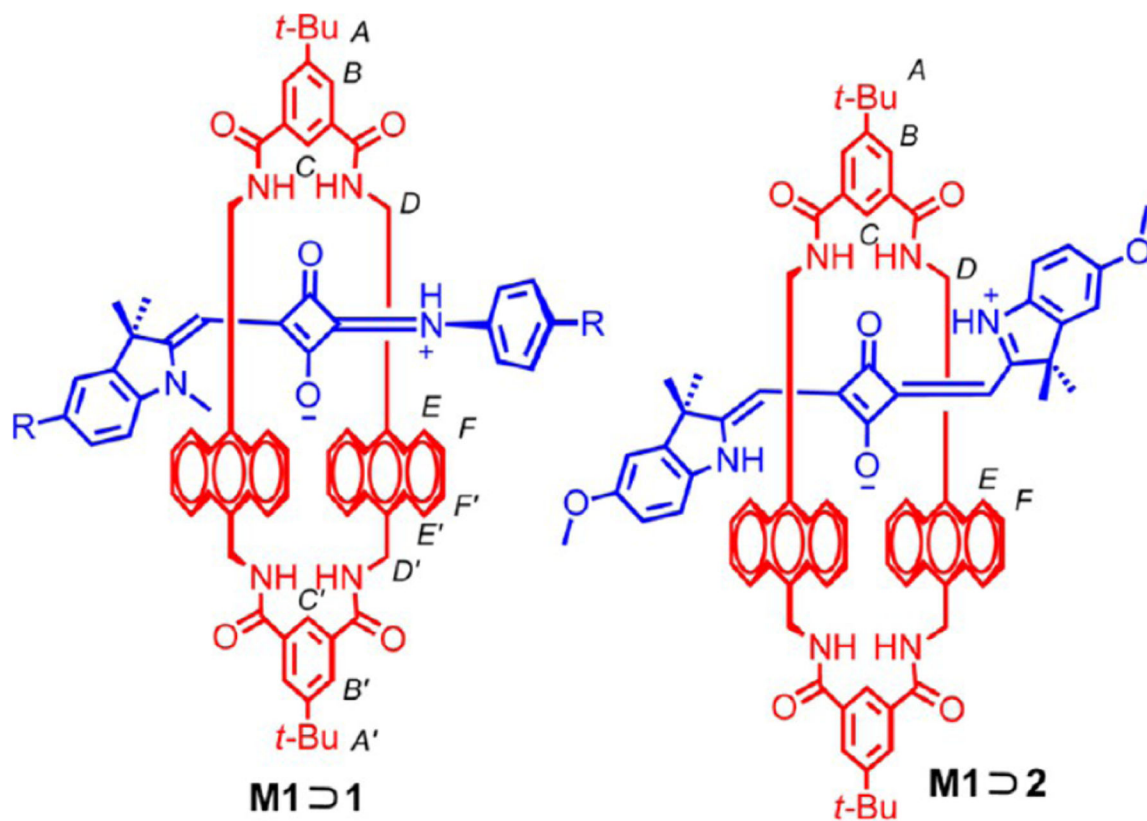
Figure 2.
Chemical structure of 3,3-dimethylindoline squaraine rotaxanes. Figure used with permission from ref 73. Copyright 2017 American Chemical Society.
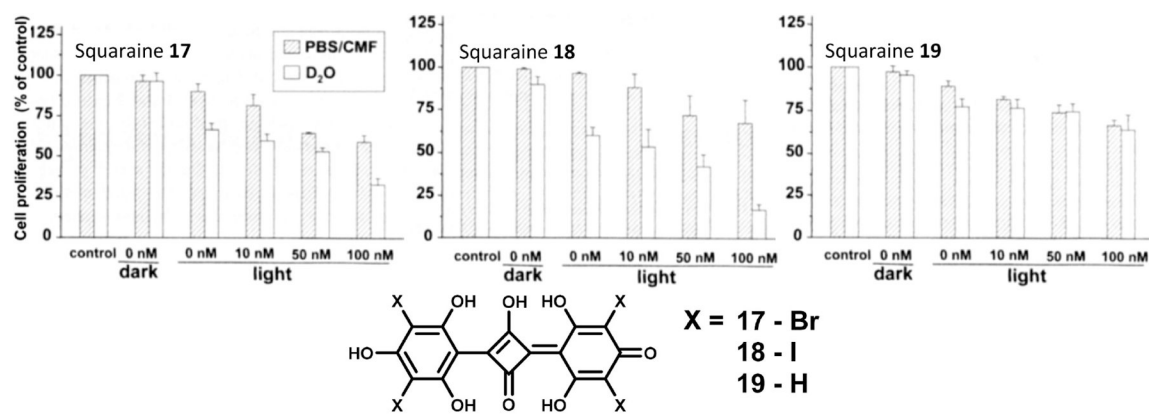
Figure 3.
Structures of squaraines **17**–**19** (bottom) and in vitro cell proliferation assays (top). Figure adapted with permission from ref 80. Copyright 2004 BioOne.
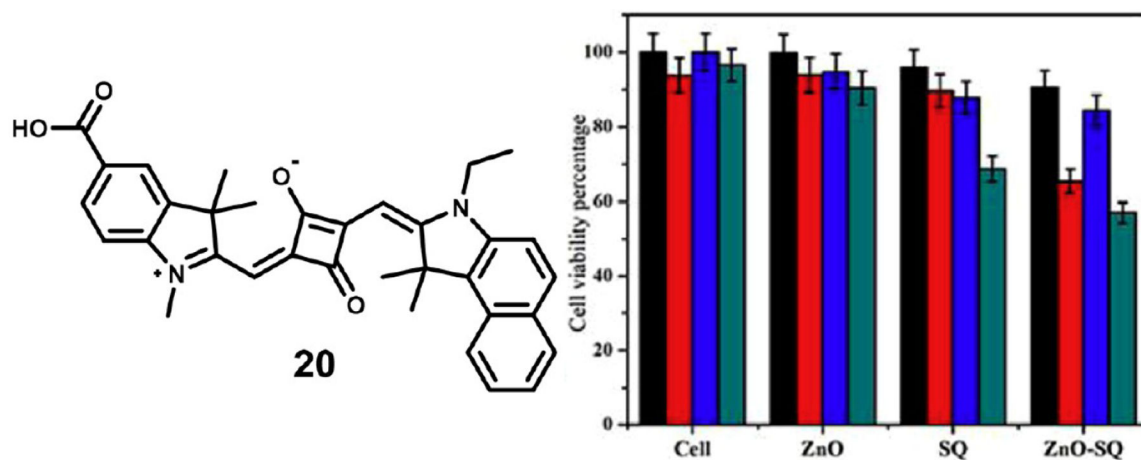
Figure 4.

Structure of squaraine **20** (left) and cell viability assay with zinc oxide nanoparticles, free squaraine dye **20**, and zinc oxide–squaraine nanohybrids showing the improved performance of the hybrid relative to the two constituents (right). Black and red bars are dark and light toxicity at 0.5 μM concentration, and blue and green bars are dark and light toxicity at 1 μM concentration. Figure adapted with permission from ref 81. Copyright 2019 Elsevier.
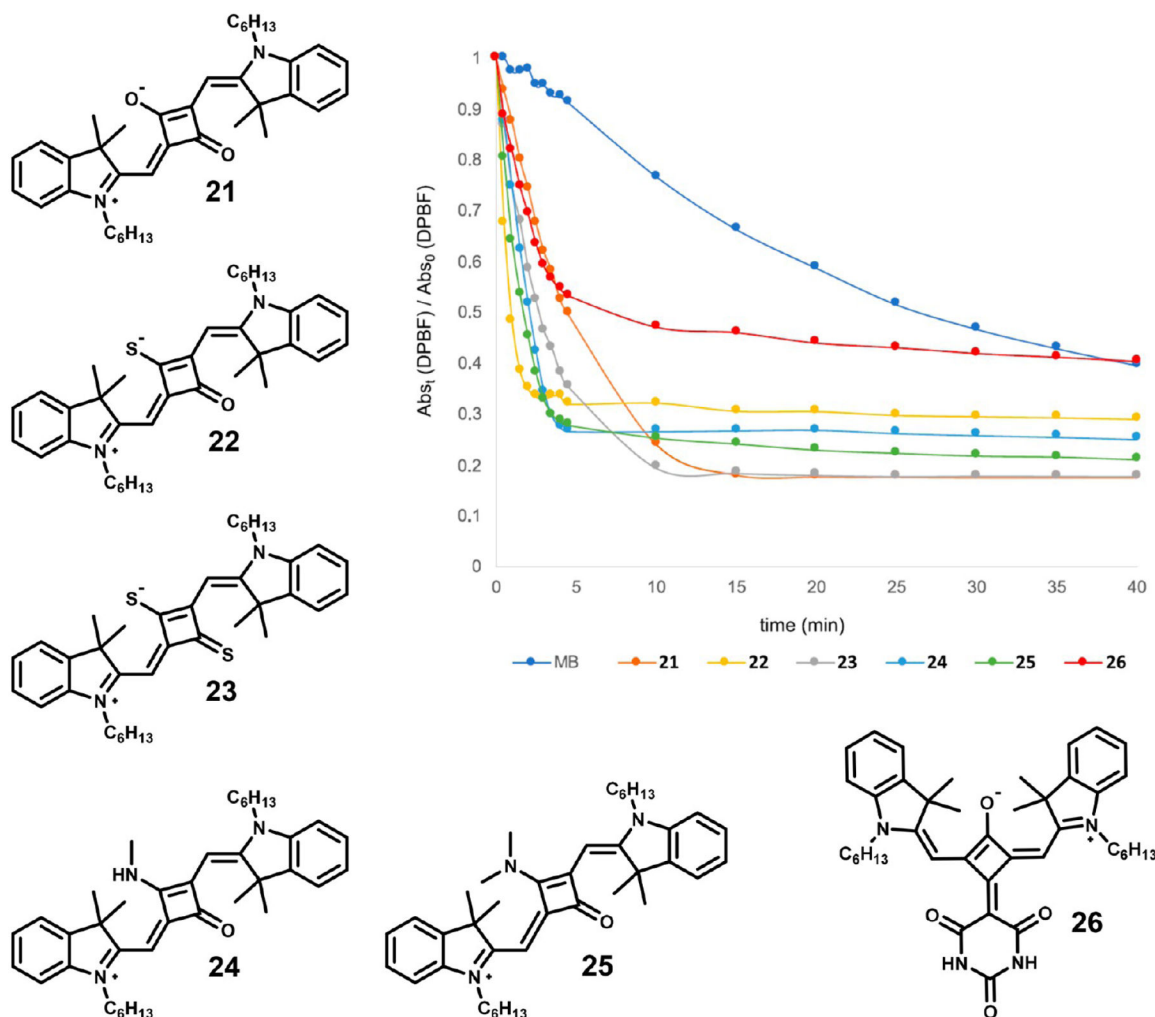
Figure 5.
Structures of squaraines **25**–**30** (left) and DPBF quantification of singlet oxygen generation during laser irradiation (right). Figure used with permission from ref 82. Copyright 2019 Elsevier.
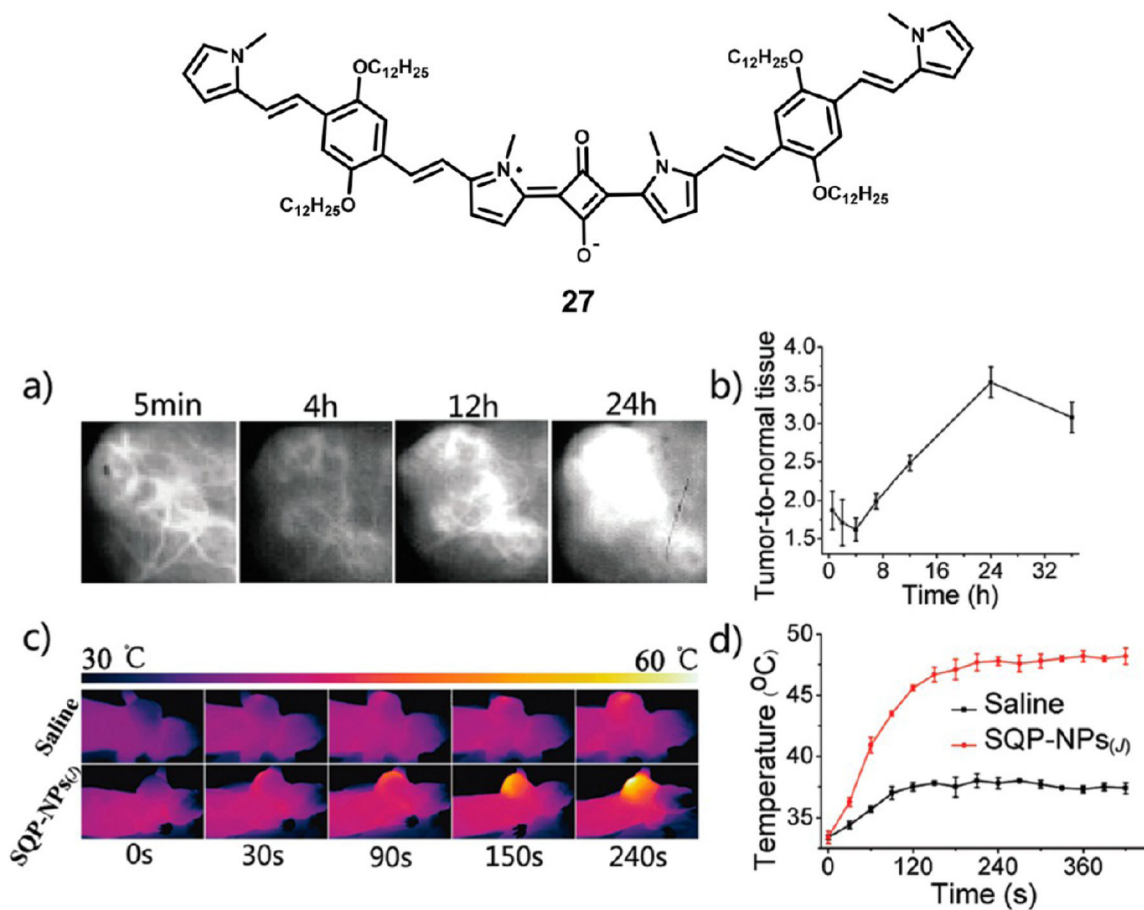
Figure 6.
Structure of J-aggregating squaraine **27** (top). Representative fluorescence images of tumor (a), tumor-to-background ratio over time (b), *in vivo* thermograph during laser irradiation (c), and temperature of tumor area during PTT (d). Figure adapted with permission from ref 89. Copyright 2018 Royal Society of Chemistry.
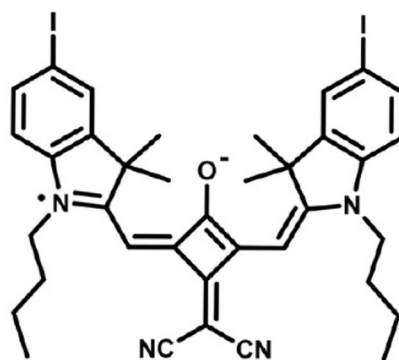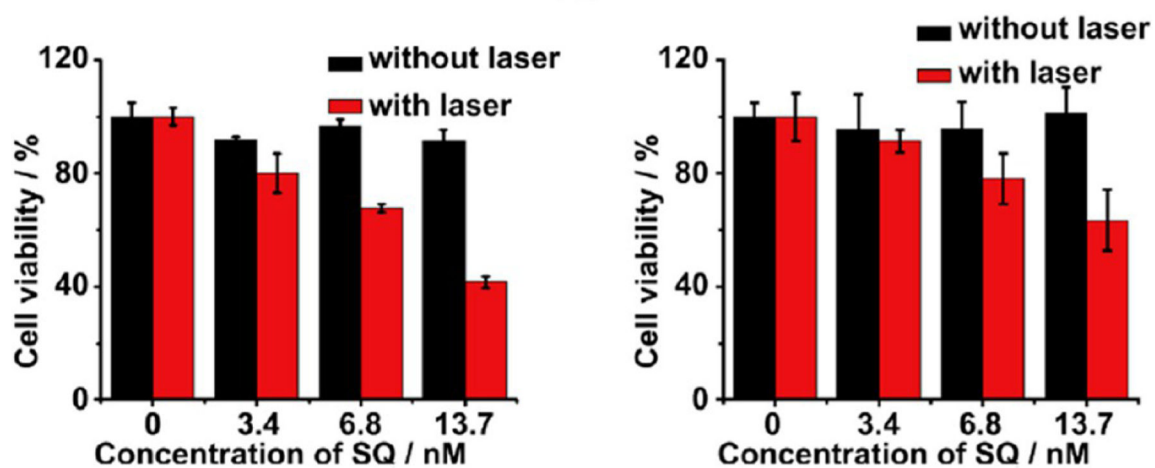
Figure 7.
Structure of squaraine photosensitizer **28** (left) and representative cell viability studies of the squaraine–BSA complex (bottom left) and folate labeled complex (bottom right). Figure used with permission from ref 90. Copyright 2014 Elsevier.
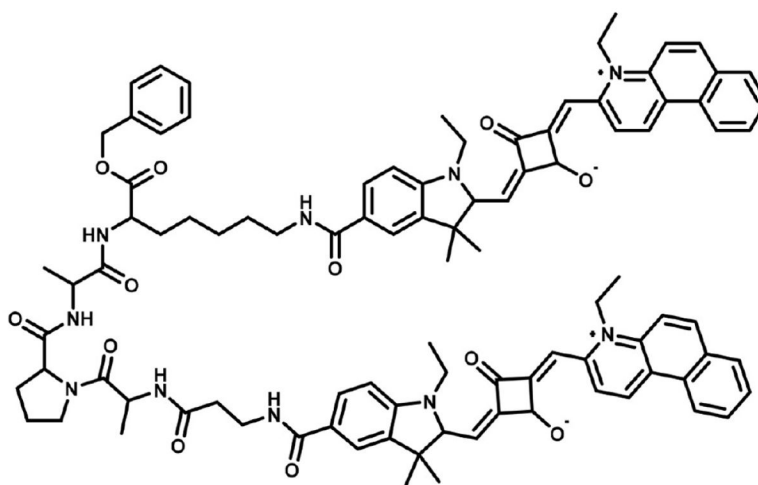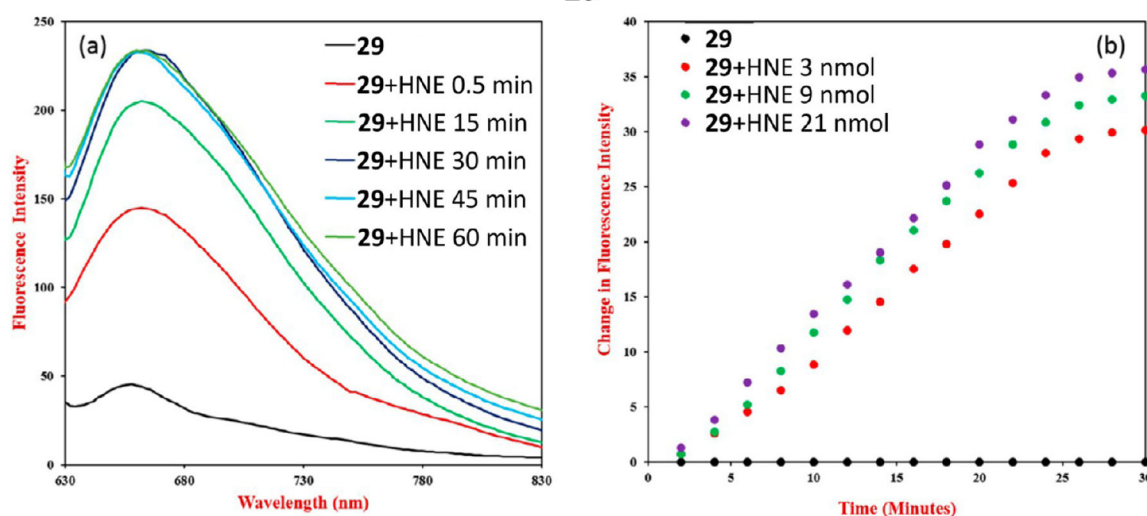
Figure 8.
Structure of squaraine conjugate **29** (top). Fluorescence spectral recovery after incubation with elastase (bottom left) and change in fluorescence intensity over time during incubation with different concentrations of elastase (bottom right). Figure adapted from ref 91 with permission. Copyright 2017 Elsevier.
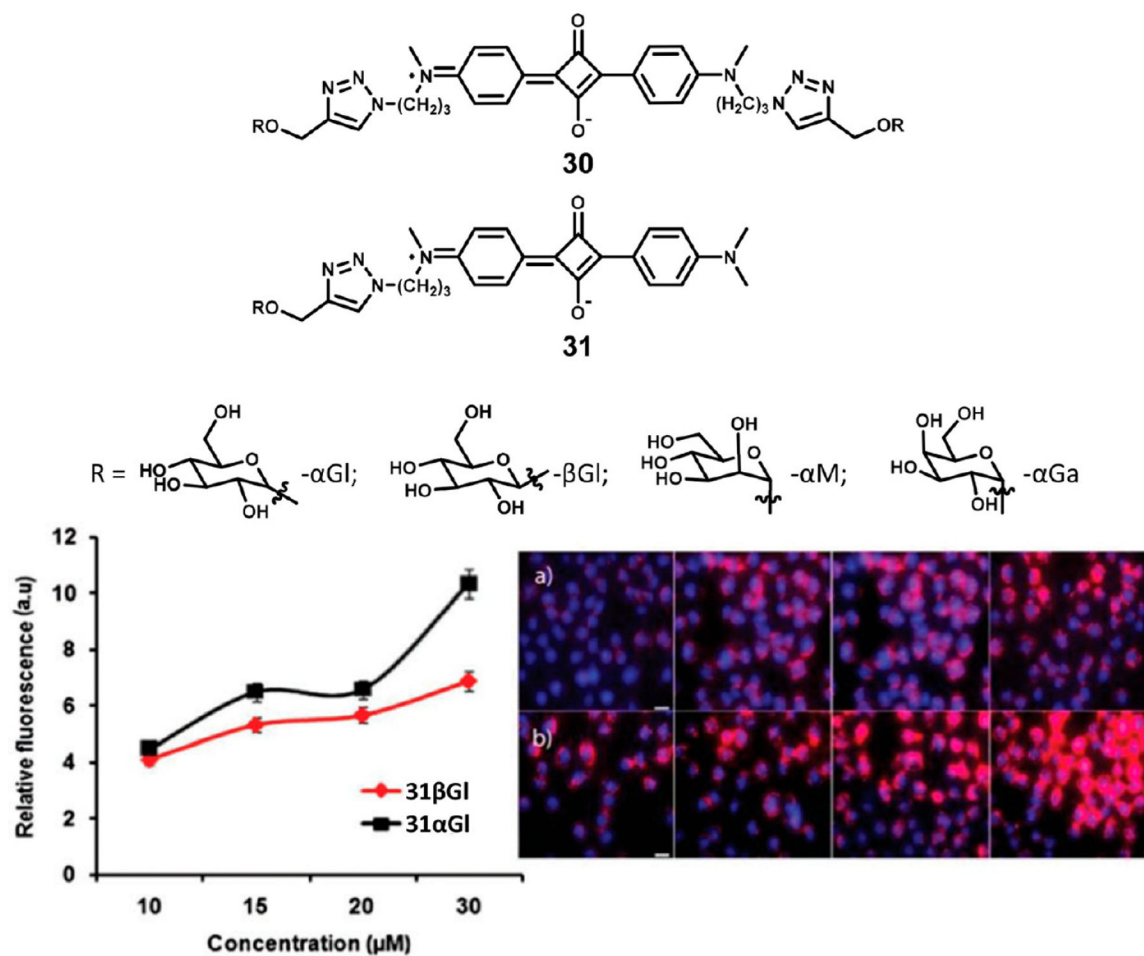
Figure 9.
Structures of carbohydrate appended squaraine dyes (top). Relative fluorescence intensity of HeLa cells incubated with increasing concentrations of (a) ASqβGl and (b) ASqαGl (bottom). Figure used with permission from ref 98. Copyright 2017 Royal Society of Chemistry.
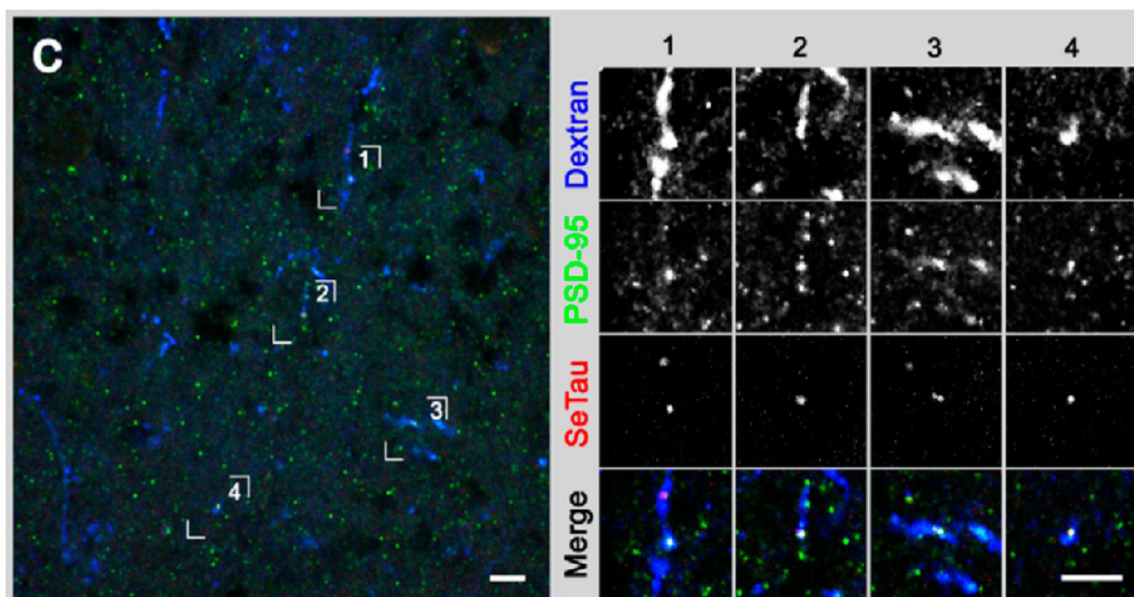
Figure 10.
Colabeling of tadpole brain with SeTau-peptide conjugate (red) and fluorescent anti-PSD-95 antibody (green) (left). In the expanded views of the highlighted regions (right), the SeTau conjugate shows strong colocalization in the neurons stained with anti-PSD-95 antibody. Cascade blue dextran was used as a space filler. Image used with permission from ref 48. Copyright 2012 Podgorski et al.
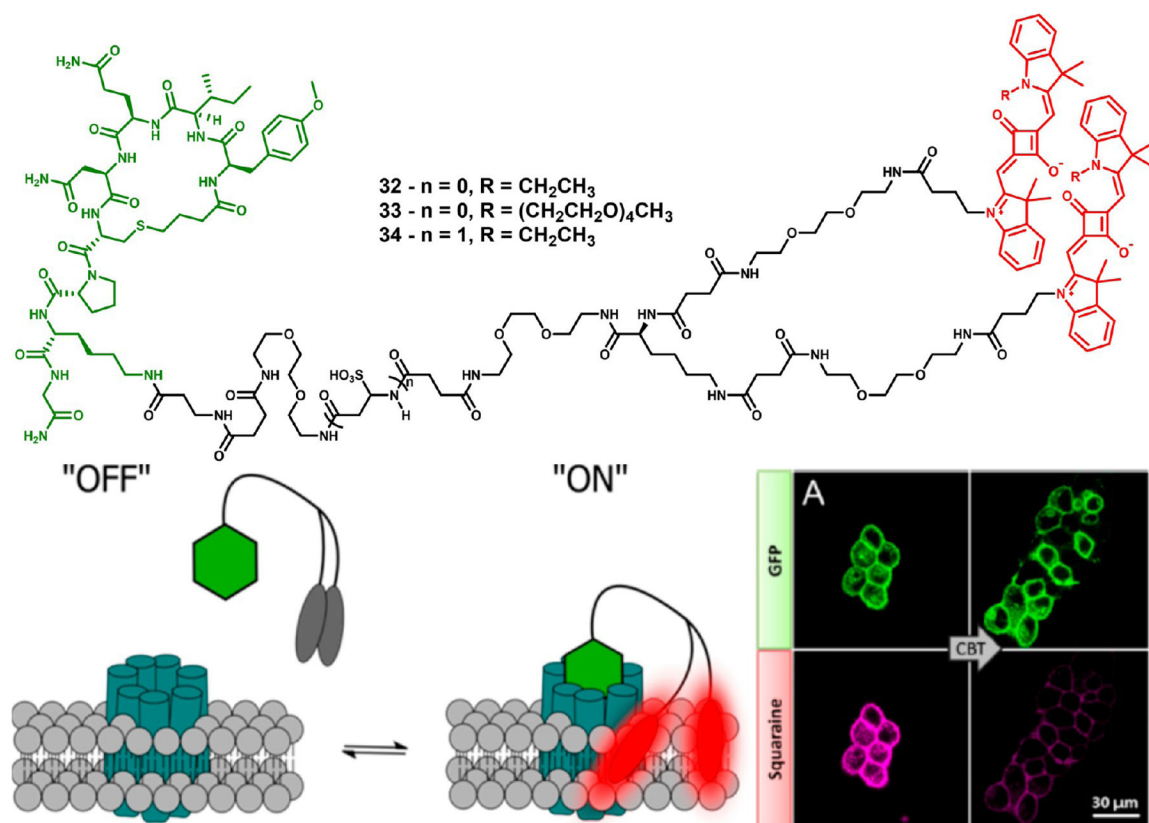
Figure 11.
Structures of squaraine dimers **32**–**34** (red) conjugated to Lys8-CBT (green) (top),
mechanism of action of dimer-based polarity sensors **32**–**34** (bottom left), and in vitro
imaging of probe **32** in GFP–OTR cells (bottom right). After addition of competing CBT,
fluorescence from the probe is significantly decreased. Figure used with permission from ref
92. Copyright 2015 American Chemical Society.

35
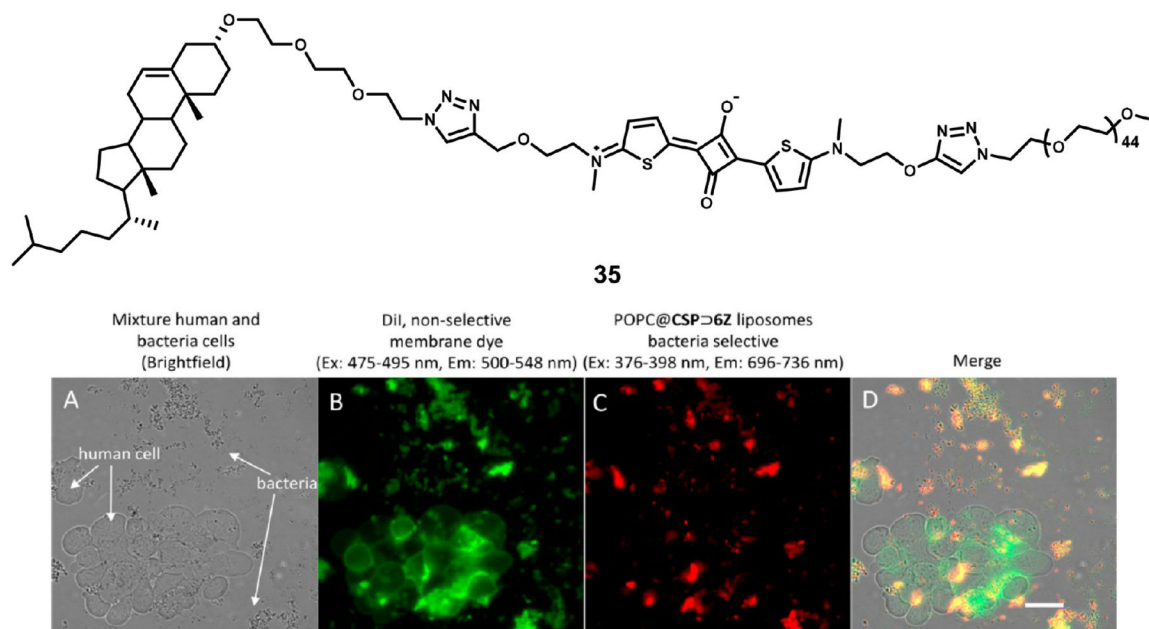
Figure 12.
Structure of CSP fluorophore **35** (top) and fluorescence microscopy of cell labeling. (A) Brightfield image of mixed human and bacterial cells, (B) fluorescence from Dil, a nonselective membrane staining dye, (C) fluorescence imaging from targeted liposomes, and (D) merge of fluorescence channels. While Dil stained both types of cells, human cells showed no red-channel fluorescence from targeted liposomes. Image used with permission from ref 100. Copyright 2017 John Wiley & Sons.
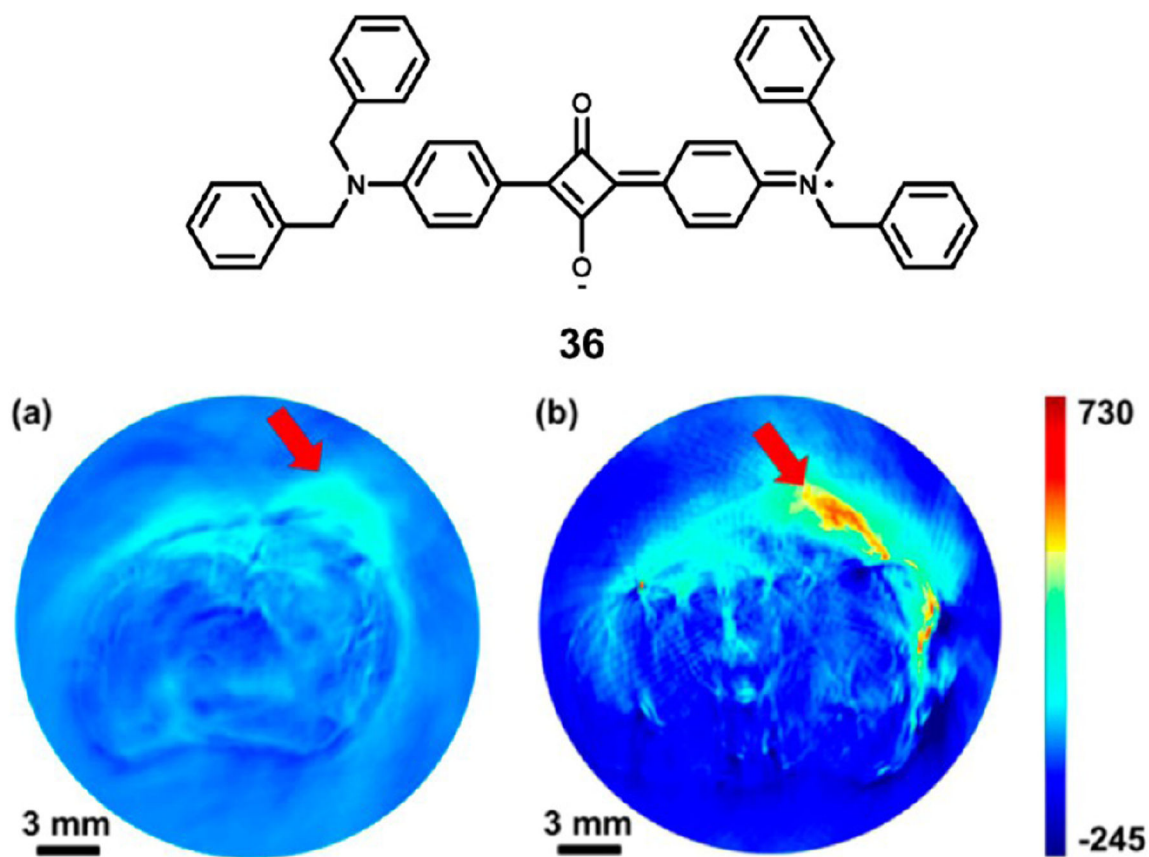
Figure 13.

Structure of squaraine **36** used in albumin nanocomplexes and *in vivo* photoacoustic tumor imaging in (a) untreated and (b) nanocomplex treated 4T1 tumor bearing mice. Image used from ref 101. Copyright 2014 American Chemical Society.
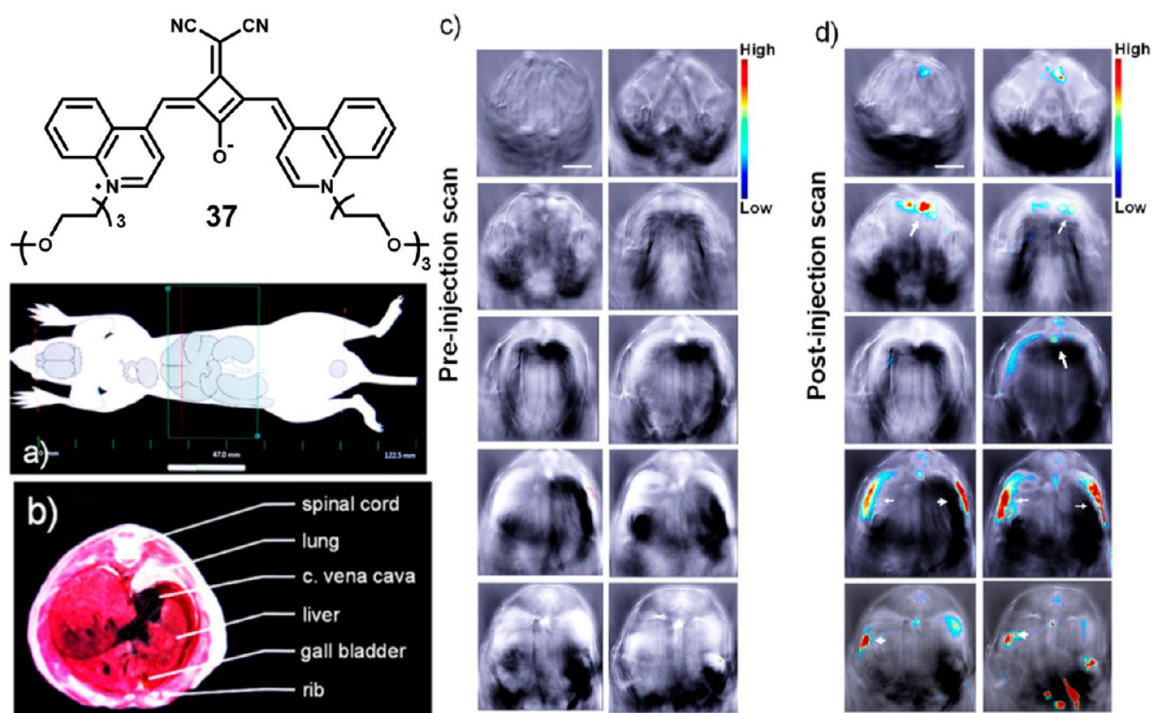
Figure 14.
Structure of micelle encapsulated squaraine **37** and representative biodistribution images. Diagram highlighting area of mouse that was imaged (a), diagram of internal anatomy of imaged area (b), and preinjection (c) and 35 min postinjection (d) optoacoustic images. Figure used with permission from ref 71. Copyright 2015 American Chemical Society.
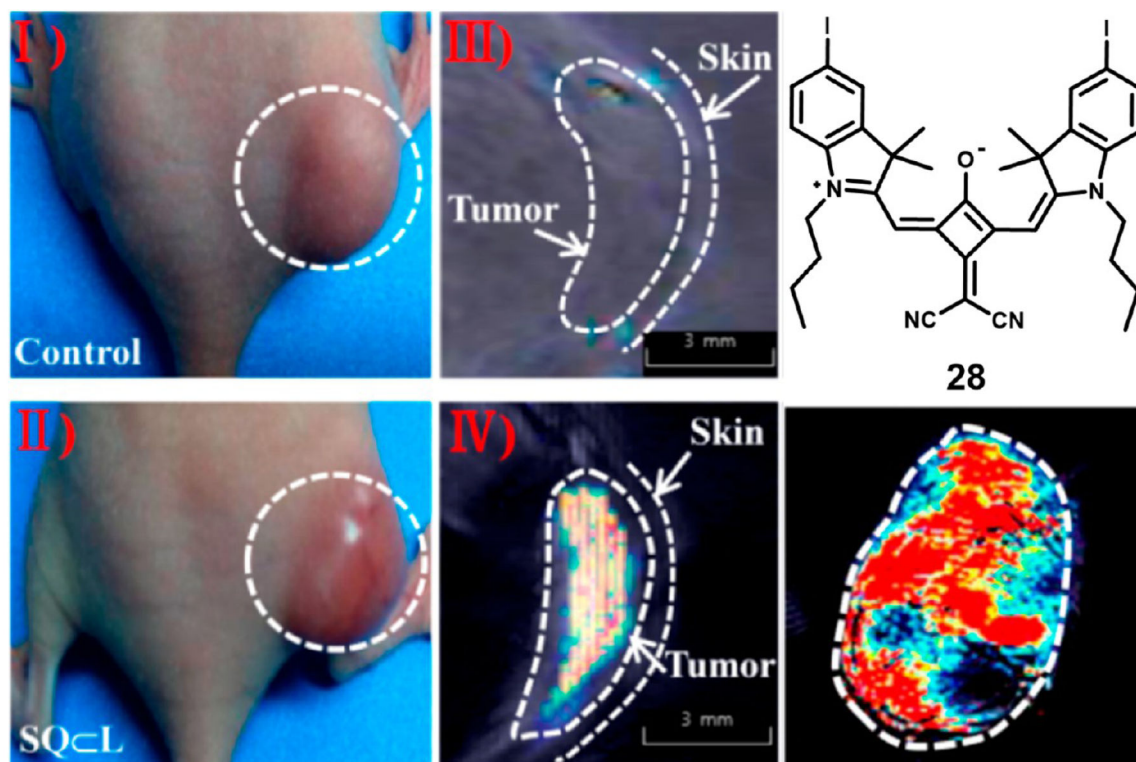
Figure 15.
In vivo MCF-7 tumor imaging with liposome encapsulated compound **28**. White light images (I and II) and optoacoustic imaging (III and IV) of tumor bearing mice (left) and optoacoustic image of resected tumor (right). Image adapted with permission from ref 102. Copyright 2014 American Chemical Society.
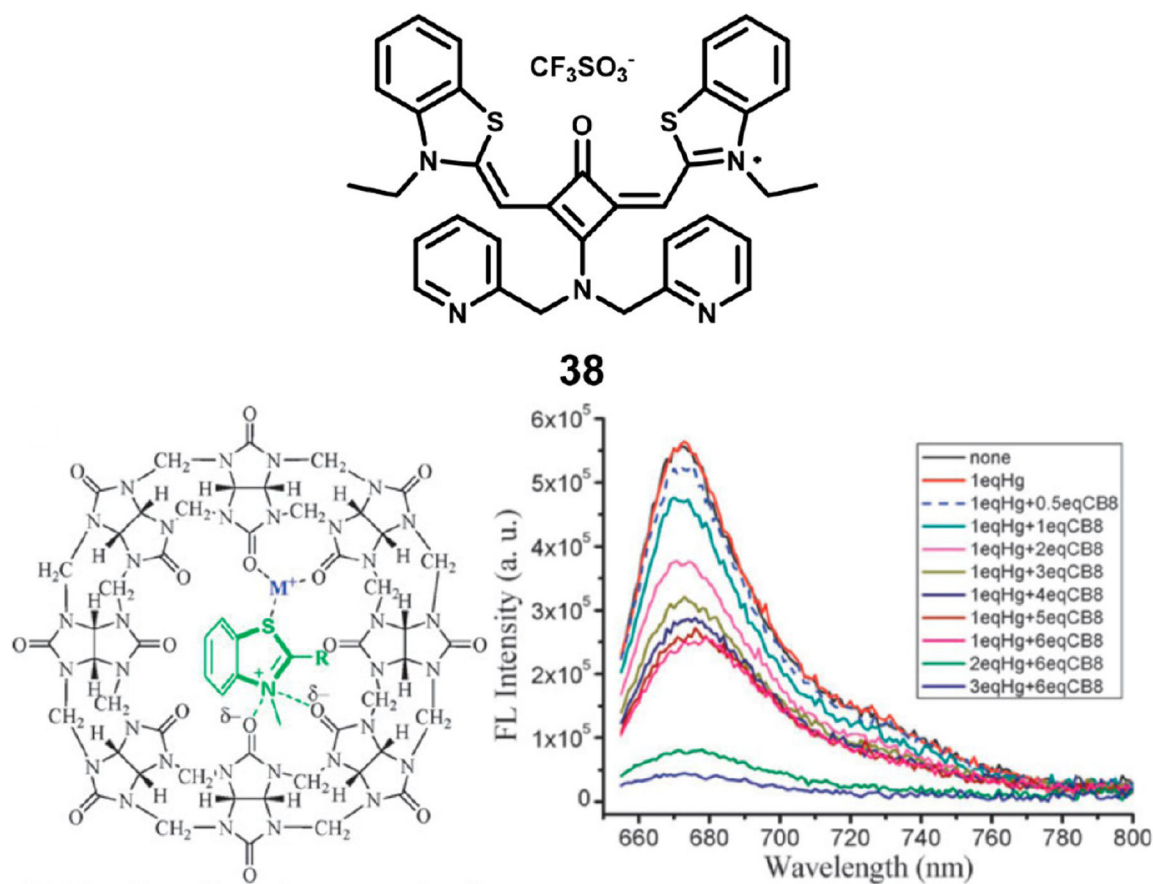
Figure 16.
Structure of squaraine **38** (top), the squaraine–cucurbit[8]uril complex with Hg^{2+} ions (bottom left), and fluorescence titration with varying equivalents of the cucurbituril macrocycle. Figure adapted with permission from ref 103. Copyright 2010 Royal Society of Chemistry.
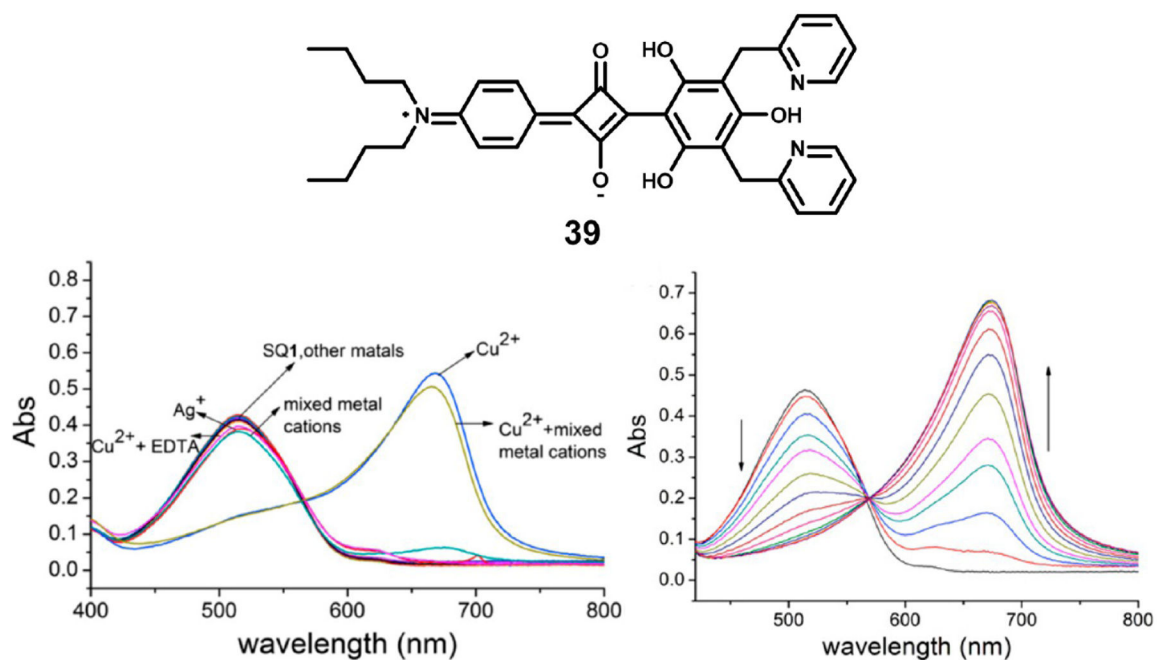
Figure 17.
Structure of squaraine **39** (top), the spectral response to various metal ions (bottom left), and absorbance spectral titration of **39** with Cu^{2+} ions. Figure used with permission from ref 104. Copyright 2010 Elsevier.
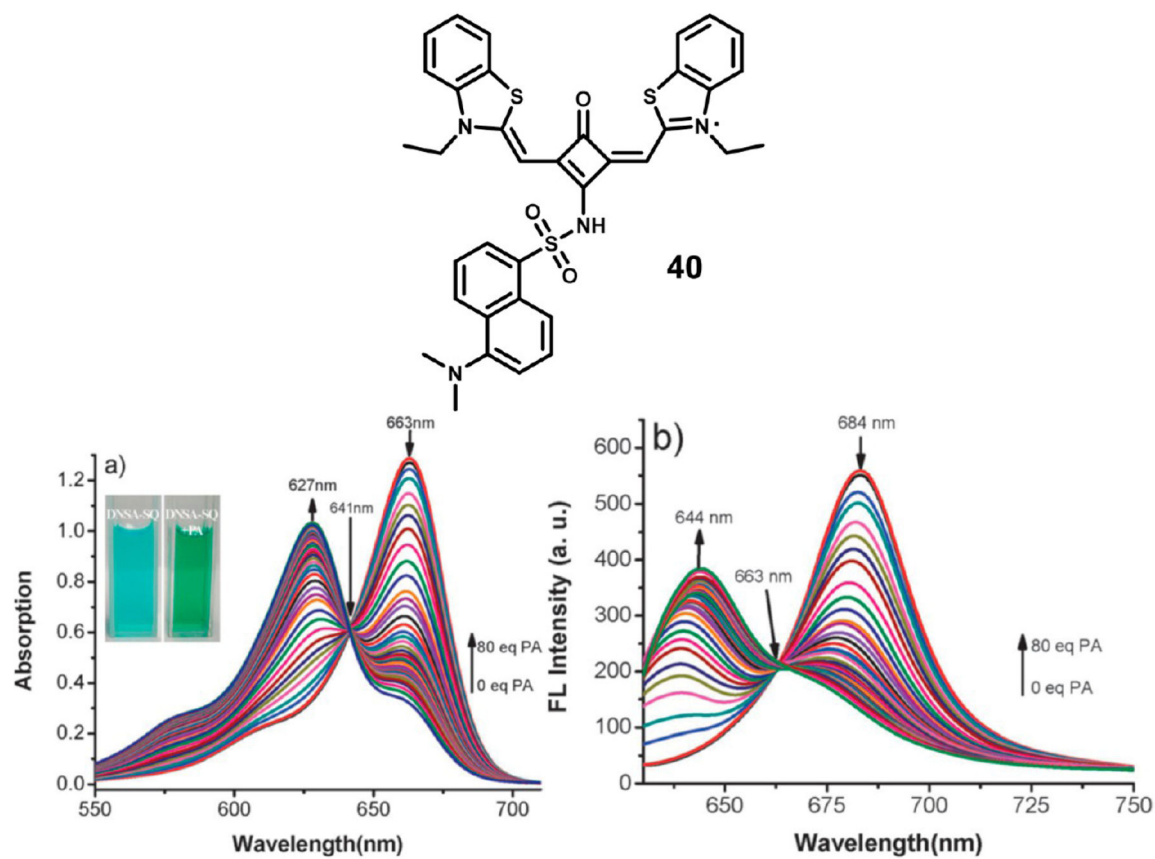
Figure 18.
Structure of dansylamide-squaraine **40** (top) and absorbance (left) and fluorescence (right) titrations with picric acid. Figures used with permission from ref 105. Copyright 2013 Royal Society of Chemistry.
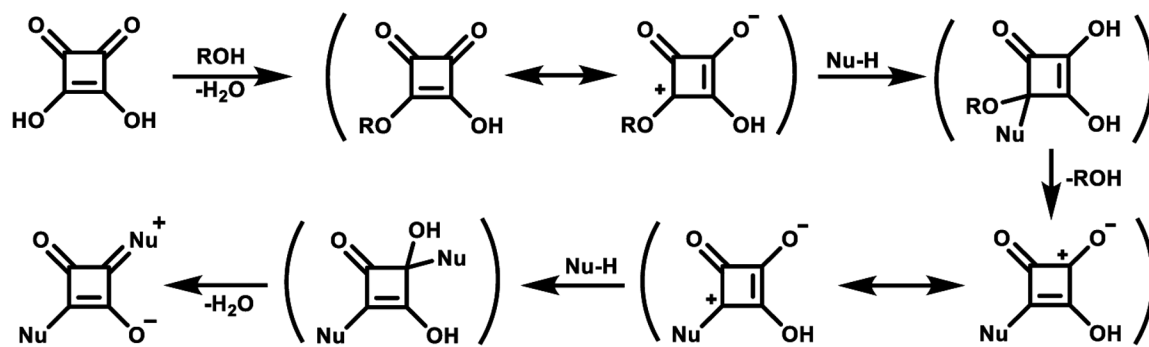
Scheme 1.
Suggested Mechanism for Symmetrical Squaraine Dye Formation[53]
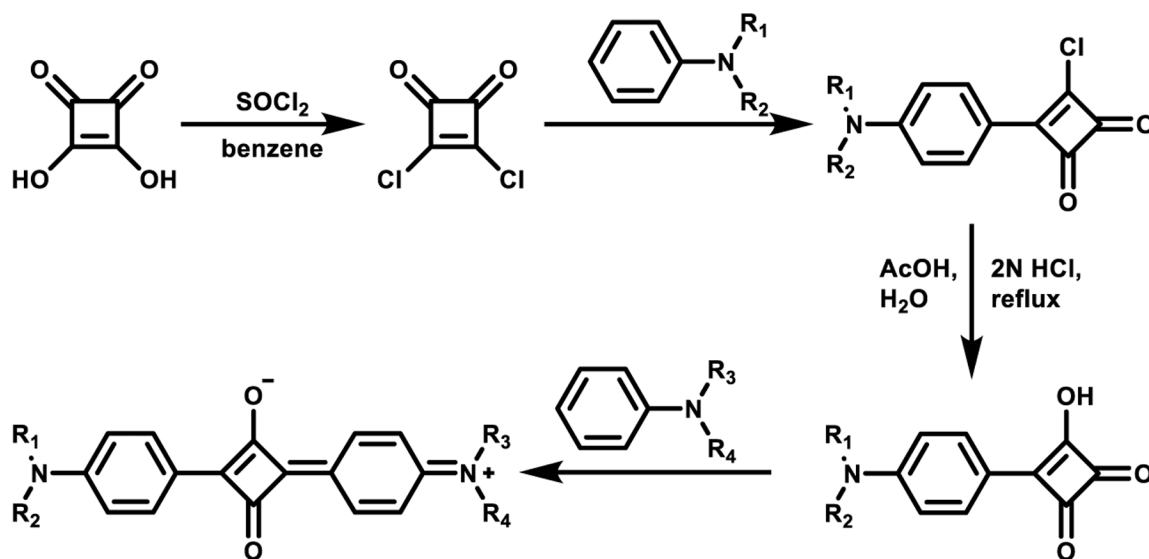
Scheme 2.
Synthesis of Unsymmetrical Squaraine Dyes Using Thionyl Chloride
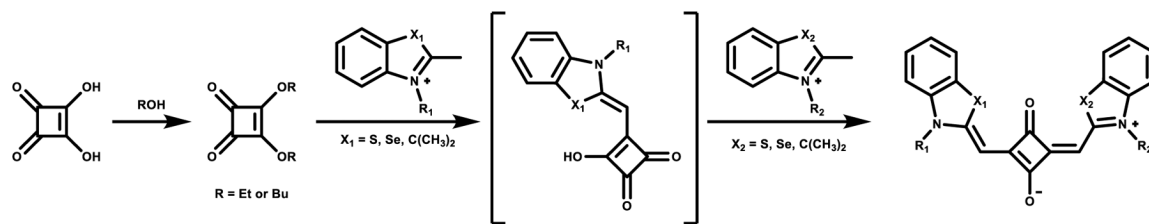
Scheme 3.
Synthesis of Unsymmetrical Squaraine Dyes with N-Alkylated Heterocyclic Structures
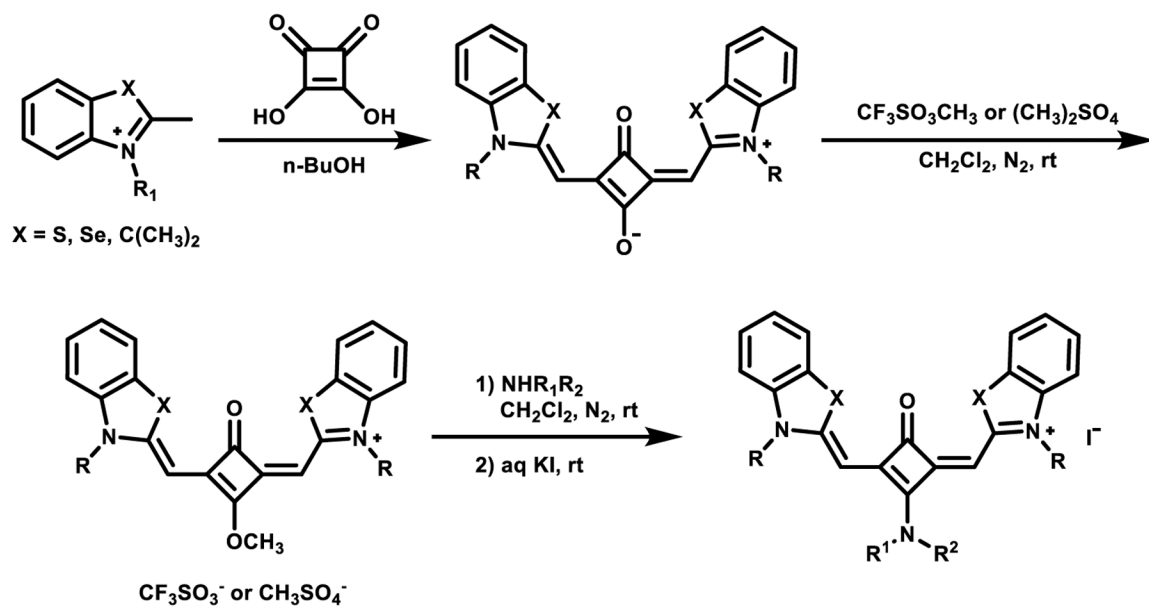
Scheme 4.
Synthesis of Aminosquaraine Dyes[60]
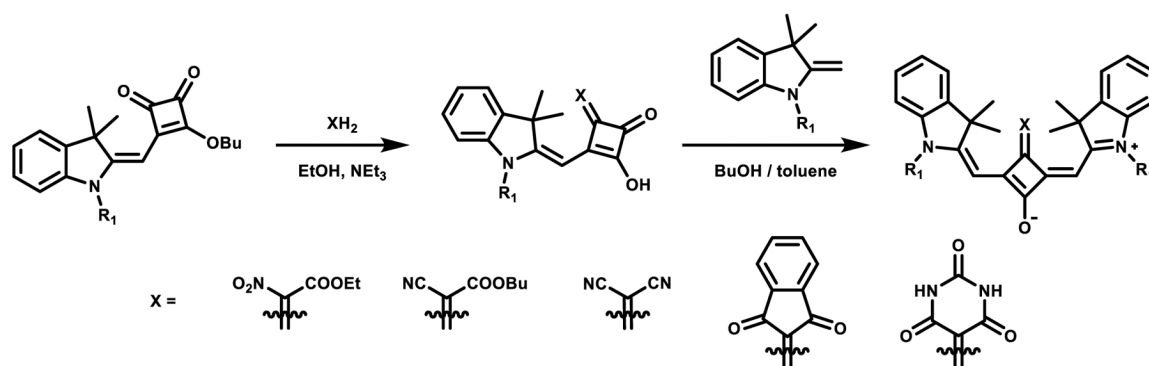
Scheme 5.
Synthesis of Some Core-Substituted Derivatives
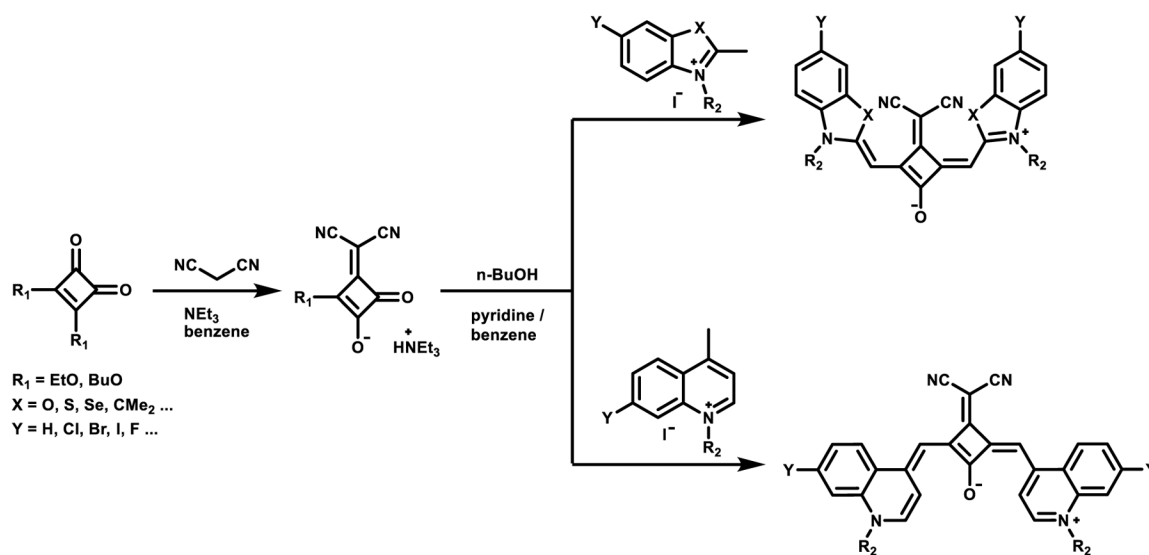
Scheme 6.
Synthesis of Symmetrical Dicyanomethylene Squaraine Dyes

Table 1.

Photophysical Properties of Squaraine Dyes in a Nonpolar Solvent (Chloroform)[66–69]
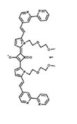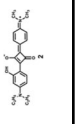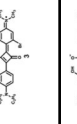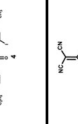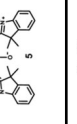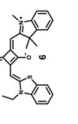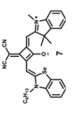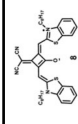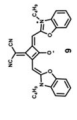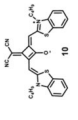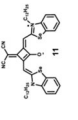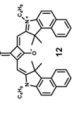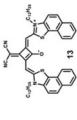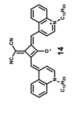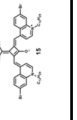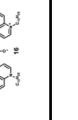
Dye structure	λ_{abs} (nm)	λ_{em} (nm)	Stokes shift (nm)	ε, ×10⁵ (M⁻¹·cm⁻¹)	Quantum yield
	684	697	13	2.80	-
	628	656	28	3.19	0.89
	632	664	32	1.20	0.81
	635	668	33	1.66	0.35
	665	687	22	1.90	0.05
	666	691	25	1.10	0.16
	677	702	25	1.80	0.26
	704	724	20	1.78	0.13

Table 2.

Photophysical Properties of Squaraine Dyes in a Polar Aprotic Solvent (DCM)[7,63,70]

Dye structure	λ_{abs} (nm)	λ_{em} (nm)	Stokes shift (nm)	e, ×10⁵ (M⁻¹cm⁻¹)	Quantum yield
9	626	646	20	1.50	0.91
10	701	720	19	1.68	0.79
11	719	737	18	1.64	0.93
12	712	722	10	2.10	0.48
13	730	747	17	1.70	0.76
14	870	890	20	2.10	0.1
15	891	916	25	2.50	0.12
16	900	920	20	2.70	0.17